Simulation of Light Interaction with Human Skin

G.V.G. Baranoski and A. Krishnaswamy

Natural Phenomena Simulation Group, School of Computer Science, University of Waterloo, Canada

Abstract

Despite the notable progress in physically-based rendering, there is still a long way to go before one can automatically generate predictable images of organic materials such as human skin. In this tutorial, the main physical and biological aspects involved in the processes of propagation and absorption of light by skin tissues are examined. These processes affect not only skin's appearance, but also its health. For this reason, they have also been the object of study in biomedical research. The models of light interaction with human skin developed by the biomedical community are mainly aimed at the simulation of skin spectral properties which are used to determine the concentration and distribution of various natural pigments. In computer graphics, the focus has been on the simulation of light scattering properties that affect skin appearance. Computer models used to simulate these spectral and scattering properties are described, and their strengths and limitations examined in detail in this tutorial. The emphasis of the discussions is on the predictive rendering of human skin, and open problems and new avenues of research in this area are also addressed.

Keywords: *skin, modeling, simulation, rendering, natural phenomena, biological imaging, medical visualization.*

Categories and Subject Descriptors (according to ACM CCS): I.3.7 [Computer Graphics]: Three-Dimensional Graphics and Realism I.3.7 [Computer Graphics]: Applications

1. Introduction

The realistic image synthesis of organic materials is still several years behind the rendering of inorganic materials. Due to limitations in this area, the generation of convincing images of organic materials, such as human skin, is usually an art entirely left to artists and animators. Computer graphics researchers and developers in the games and entertainment industries can certainly benefit from being able to automatically generate realistic images of organic materials through the use of predictive reflectance and scattering models.

On the biomedical side, the investigation of the processes of light interaction with human skin can lead to the development of more accurate noninvasive protocols to automatically diagnose medical conditions such as jaundice (yellowish hue), erythema (redness) [96] as well as tumors at early stages [28]. The importance of such biomedical applications is highlighted by the fact that a significant number of people is affected by these medical conditions and skin related diseases. For example, in the United States, more than 50,000 new cases of melanoma, the most serious form of skin cancer, are reported to the American Cancer Society each year [129]. Furthermore, the understanding of the mechanisms involved in the processes of light propagation and absorption in skin tissues is central for the development of lotions protective against harmful solar radiation as well as the design of superior cosmetics.

This tutorial discusses the recent advances in the simulation of light interaction with human skin. In particular, it addresses the processes of light transport and absorption in skin tissues, and examines computer models used to simulate these natural phenomena. In addition to the direct contributions to the realistic and predictive simulation of skin appearance, the algo-

rithms used in models of light interaction with human skin can be extended to models aimed at the rendering of other organic materials such as hair, fur, leaves, petals and ocular tissues.

It is important to note that there are several subsurface scattering models in the graphics literature which are neither biologically motivated nor specifically designed to simulate light interaction with human skin (*e.g.*, plants [10] and hair [81]). An extensive review of these models is beyond the scope of this tutorial, and the interested reader can find more information in a recent survey by Premoze [107]. In addition, there has also been recent works in image based techniques for rendering and altering the appearance of skin [55, 137], which do not address the modeling of light propagation and absorption in skin tissues, and for this reason are not examined in this tutorial.

The remainder of this tutorial is organized as follows. It continues with a review of optics and appearance concepts used in the design and validation of models of light interaction with organic matter (Section 2), followed by a presentation of biological factors involved in the processes associated with light propagation and absorption in skin tissues (Section 3). These processes have been extensively studied by the biomedical community since they also affect the health of skin tissues. The models developed in this field are, however, mostly aimed at the reproduction of skin spectral properties to determine the content and distribution of various substances, *i.e.*, scattering properties affecting skin appearance are usually not addressed. In computer graphics, on the other hand, the focus has been on developing scattering models to be used in image synthesis frameworks. Nevertheless, these models incorporate algorithms and techniques used in biomedical models. More recently, research efforts have been directed toward the development of models that take as input biological data and compute both spectral and scattering quantities for skin specimens. Taking into account these aspects, this tutorial provides a review of the most important modeling approaches used in biomedical applications (Section 4) followed by a more detailed examination of current models used in image synthesis frameworks (Section 5-8). The tutorial will conclude with a discussion of open problems and current trends in the predictive rendering of human skin (Sections 9 and 10).

2. Light, Optics and Appearance

In this section we review fundamental aspects of light interaction with matter, including the definition of optics and radiometric quantities used throughout the tutorial.

2.1. Light as Radiation

Light is a form of energy, which includes not only the visible light[†], but also other forms of electromagnetic radiation such as microwaves and X-rays (Figure 1). The parameter used to distinguish among the different types of radiation is the wavelength, λ, which is usually measured in nanometers (nm, $10^{-9}m$). Light can be considered to behave like waves or particles.

In 1900, Planck demonstrated that matter does not emit light continuously as it was predicted by the electromagnetic theory of Maxwell. Instead, according to Planck, light is emitted as small packets of energy, or *quanta*. This idea that energy comes only in discrete quantities is considered the beginning of quantum mechanics, a revolutionary theory for submicroscopic phenomena [56], and it is also essential for the understanding of light interactions with matter. In 1905, building on Planck's idea, Einstein postulated that energy along an incident beam is quantized into "particles", later called *photons* [78], whose individual energy is given in terms of their wavelength and Planck's constant [50, 56].

The concept of photons is fundamental for geometrical optics [56, 79], also called ray optics, which involves the study of the particle nature of light. In geometrical optics the large-scale behavior of light, such as reflection and refraction, is described by assuming light to be composed of non-interacting rays, each of them carrying a certain amount of energy.

Also in 1905, Schuster [114] published a paper on radiation through a foggy atmosphere, and later, in 1906, Schwarzschild published a paper on the equilibrium of the Sun's atmosphere [88]. These two astrophysical works are considered the beginning of the radiative transfer theory [5, 22, 106]. This theory combines principles of geometrical optics and thermodynamics to characterize the flow of radiant energy at scales large compared with its wavelength and during time intervals large compared to its frequency [5].

There are phenomena at the level of electromagnetism, such as interference[‡], diffraction[§] and polar-

[†] In 1704, Isaac Newton observed that the visible white light could be split by a glass prism into a rainbow of colors which could not be further subdivided.

[‡] The term interference refers to the phenomenon that waves, under certain conditions, intensify or weaken each other [90].

[§] In this context diffraction refers to the slight bending of

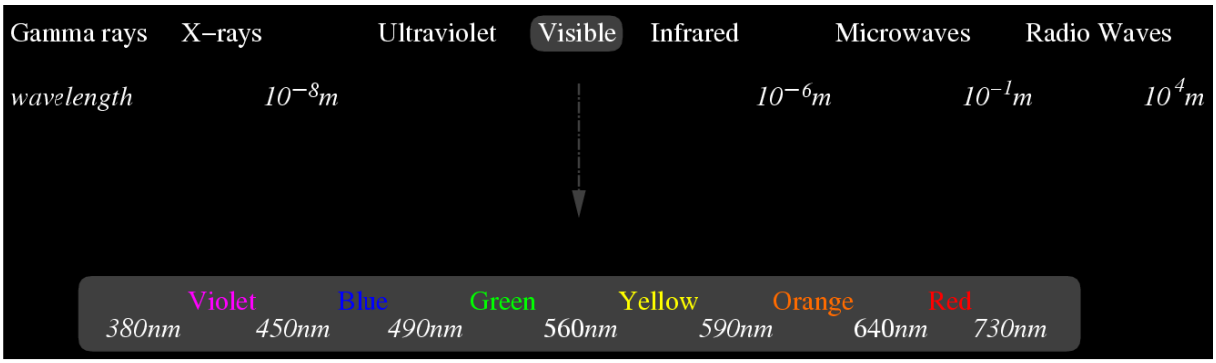

Figure 1: *Abridged chart describing the electromagnetic spectrum of light.*

ization[¶], that cannot be explained by geometrical optics or radiative transfer theory. These phenomena are addressed by physical optics [56, 79], which involves the study of the wave nature of light. Despite this limitation, geometrical optics and radiative transfer theory are the two levels of physical description largely used in the simulation of visual phenomena aimed at image synthesis applications. As mentioned by Glassner [50], this is a pragmatic choice, since the simulation of phenomena such as interference, diffraction and polarization usually requires enormous computational resources to produce results of significantly higher error fidelity and complexity than those attainable by geometrical optics.

From a practical point of view, it is more efficient to model light as rays rather than waves. We can think of a wave as just a ray with an energy, and the wavelength of light, a physical optics parameter important for rendering applications, can be included in geometrical optics by associating a wavelength with each ray [119]. Furthermore, as pointed out by Shirley [119] and Arvo [5], physical or wave optics phenomena have a small visual role in most computer graphics applications. For instance, the light sources commonly used in rendering are usually incoherent, and effects related to phase, such as interference, are usually masked [5]. Also, diffraction phenomena are noticeable for long wavelength radiation, but have a fairly small effect for visible light [119].

Furthermore, in computer graphics it is usually assumed that the energies of different wavelengths are decoupled. In other words, the energy associated with some region of the space, or surface, at wavelength λ_1 is independent of the energy at another wavelength λ_2 [50].

2.2. Light Interactions with Matter

The problem of determining the appearance of an object or an environment involves the simulation of light interactions with matter, which, in turn, involve three main processes: emission, scattering and absorption.

2.2.1. Emission

Man made and natural light sources emit light with characteristic spectral distributions, which depend on the nature of the emission process. The processes of light emission can be divided into two types: thermal and luminescent [50].

Thermal emissions are due to the material radiating excess heat energy in the form of light. For these materials, called thermal radiators, the amount of light emitted is primarily dependent on the nature of the material and its temperature. For example, an incandescent light bulb is a thermal radiator where an electric current is run through the filament to make it hot, and the filament gets rid of the heat by dispersing the energy through the emission of particles in a range of energy. An ideal thermal radiator of uniform temperature whose radiant exitance in all parts of the spectrum is the maximum obtainable from any thermal radiator at the same temperature is called a *blackbody* [‖] [59]. Although no material reaches the theoretical maximum of a blackbody, it is sometimes convenient to describe the emissive properties of a material by specifying, on a wavelength-by-wavelength basis, the

light that occurs when light passes very close to an edge [98].

[¶] Polarization of light refers to having the electrical portion of the light waves moving in a single direction rather than in random directions [98].

[‖] The designation blackbody is appropriate because such a body will absorb all incident flux [59].

fraction of light it generates with respect to a blackbody [50]. For example, solar radiation arrives at the Earth's atmosphere with a spectral energy distribution similar to a blackbody radiator of $5,800°K$ (Figure 2) [123].

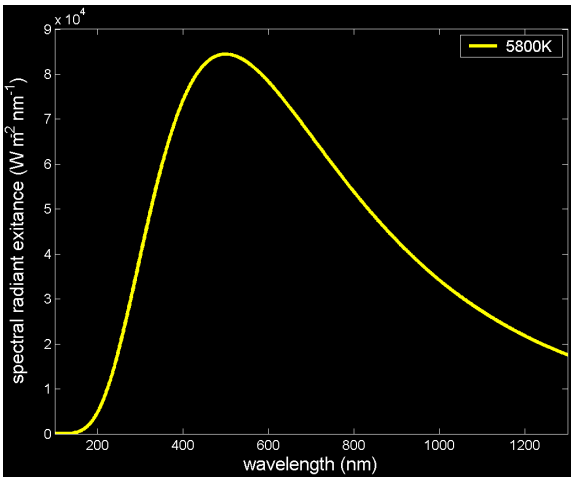

Figure 2: *Spectral energy distribution of a blackbody radiator of* $5,800°K$.

Luminescent emissions are due to energy arriving from elsewhere, which is stored in the material and emitted (after a short period of time) as photons. The incident energy, primarily due to factors other than temperature, causes the excitation of electrons of the material. These electrons in the outer and incomplete inner shells move to a higher energy state within the atom. When an electron returns to the ground state a photon is emitted. The wavelength of the emitted photon will depend on the atomic structure of the material and the magnitude of the incoming energy. Ordinarily an electron remains in its excited state for about 10^{-9} seconds [153]. If there is a much longer delay and the electron emits a photon in the visible range, having being originally excited by a photon of differing wavelength, the process is called phosphorescence. The distinction between phosphorescence and fluorescence is a matter of scale (time).

A phosphor is defined as a luminescent material that absorbs energy and reemits it over some period of time, which is associated with the lifetime of the excited electron. Most phosphors are inorganic, *i.e.,* carbon-free, crystals that contain structural and impurity defects. Examples of these materials are used in TV screens and computer monitors (CRT).

As described by Williamson and Cummings [153], atoms can be excited in many ways other than absorbing a photon. The term "phosphorescence" was originally applied to light given off by the reactive element phosphorous and chemically similar substances when left exposed to air. They spontaneously combine with oxygen in a slow reaction and in the process emit light. This process of light emission as a result of a chemical reaction is called chemiluminescence [153]. A related effect is bioluminescence, when light is produced by chemical reactions associated with biological activity. When one hard object is sharply struct against another we may observe a "spark" or light emission termed triboluminescence. Excitation is also possible due to the impact of high energy particles, which may cause impressive light emissions such as those found in aurorae and space nebulae.

2.2.2. Scattering

The three main types of scattering occurring in Nature are the following: Mie, Rayleigh and reflective-refractive scattering. Mie, or aerosol, scattering occurs when the wavelength of the radiation is comparable to the size of the molecules, or particles, through which is passing. Rayleigh, or molecular, scattering occurs when the wavelength of the radiation is somewhat larger than the molecules, or particles[**], through which it is passing. It is proportional to the fourth power of the frequency, and hence the shorter wavelengths are preferentially attenuated. As the particles get larger, scattering tends to be more uniform across the spectrum [123]. Reflective-refractive accounts for most of the internal scattering occurring in organic tissues such as plant leaves and human skin. It is mainly caused by the arrangement of tissues, and the refractive differences, which, for the most part, are associated with air-cell wall interfaces with respect to cells whose dimensions are quite large compared with the wavelength of light. Due to its dependency on the refractive differences, the variations across the spectrum are directly associated with the wavelength dependency of the refractive indices of the materials.

2.2.3. Absorption

Once light is transmitted into a medium, it may be absorbed. In a dielectric, this will happen if there are absorptive elements, such as dye or pigments, inside the medium. Pigments are materials that exhibit selective reflection and selective absorption [50], while dyes exhibit some luminescence produced due to excitation. The spectral distribution of the light due to the absorption process depends on the distribution, concentration and specific absorption coefficient (s.a.c.)

** The error in applying Rayleigh, rather than Mie, theory to small particles is less than 1% when the radius of the particle is smaller or equal to 0.03λ [85].

of the absorptive elements. The s.a.c. of a natural pigment can be obtained by dividing its molar extinction coefficient by its molar weight. For example, the s.a.c. of β-carotene, a natural pigment present in plants and human skin, is given by:

$$\zeta(\lambda)_{car} = \frac{\varepsilon_{car}(\lambda)}{537} \quad (1)$$

where:
$\varepsilon_{car}(\lambda)$ = molar extinction coefficient of β-carotene $(cm^{-1}/(moles/L))$,
537 = molecular weight of β-carotene $(g/mole)$.

The s.a.c. curves may be adjusted according to the lengthening of the optical path of a tissue, also called ratio of intensification [21] or factor of intensification [110]. This factor represents a combination of light that passes through tissues without encountering an absorber (sieve effect) and the light that is scattered and has an increased path length (detour effect). As mentioned by Vogelmann [149], these two phenomena have opposite outcomes: the sieve effect lowers absorption (specially at or near wavelengths for which the absorption has a maximum value), whereas the detour effect increases absorption (specially at or near wavelengths for which the absorption has a minimum value). Nonetheless, the absorption may be enhanced in dispersive samples by the combination of these two effects [110].

Inorganic dielectrics like pure water absorb light, but the absorption can be considered negligible in the visible portion of the light spectrum. Metals may also absorb transmitted light. Although they are usually opaque, thin metal coatings, such as the gold film on some sunglasses, can be partially transparent [119].

2.3. Tissue Optics Definitions and Terminology

A modeling approach commonly applied in tissue optics considers organic tissues to be a random turbid media which have volumetric scattering and absorption properties [103]. These properties are represented by the volumetric absorption and scattering coefficients[††].

The absorption coefficient is obtained by multiplying the absorption cross section of an absorber particle by the density of the absorbers in the medium [60]:

$$\mu_a = \frac{C_a(\lambda)\ v_a}{V} \quad (2)$$

where:
$C_a(\lambda)$ = absorption cross section,
v_a = volume fraction of of absorbers,
V = volume.

Similarly, the scattering coefficient is obtained by multiplying the scattering cross section of a scatterer particle by the density of the scatters in the medium [60]:

$$\mu_s(\lambda) = \frac{C_s(\lambda)\ v_s}{V} \quad (3)$$

where:
$C_s(\lambda)$ = scattering cross section,
v_s = volume fraction of scatters,
V = volume.

The sum of scattering and absorption coefficients gives the attenuation coefficient (μ). These coefficients are typically measured in inverse length units, while the cross sections are given in area units. The absorption cross section of a particle corresponds to the total power absorbed by the particle, and it is a function of the orientation of the particle and the state of polarization of the incident light [143]. Similarly, the scattering cross section of a particle corresponds to the total power scattered by the particle, and it is also a function of the orientation of the particle and the state of polarization of the incident light [143]. The complete derivation of cross section expressions is beyond the scope of this tutorial, and the interested reader is referred to the texts by van de Hulst [143] and Bohren and Huffman [17].

It is worth noting that in tissue optics these coefficients are usually used to describe the optical properties of whole tissues instead of their basic constituents. This approach may introduce undue inaccuracies in the simulations since these coefficients are usually determined using inversion procedures (Section 4), and there is a noticeable scarcity of direct measured data.

Three other parameters are commonly used to simulate light propagation in a tissue assumed to be a random medium with volumetric properties: albedo, optical depth and phase function. The albedo is a dimensionless parameter defined as the ratio between the scattering coefficient and the attenuation coefficient:

$$\gamma(\lambda) = \frac{\mu_s(\lambda)}{\mu(\lambda)} \quad (4)$$

The optical depth represents the product of the tis-

[††] Usually the term volumetric is omitted.

sue thickness and the attenuation coefficient [103]:

$$\varrho(\lambda) = h\ \mu(\lambda) \tag{5}$$

An optical depth of 1 indicates that there is a probability of approximately 33.78% that light will traverse the tissue without being neither scattered nor absorbed [103], *i.e.*, the ratio between the incident and the transmitted power corresponds to:

$$\frac{\Phi_t(\lambda)}{\Phi_i(\lambda)} = e^{-\varrho(\lambda)} = e^{-1} = 0.3678$$

When light hits a particle with an index of refraction different from that of its environment, the light is scattered. The direction of scattering is characterized by the polar angle θ at which the light is bent and an azimuthal angle β in a plane normal to the direction of incidence (Figure 3). A phase function denoted by $\Gamma(\theta, \beta)$ describes the amount of light scattered from the direction of incidence to the direction of scattering [143], *i.e.*, it represents a single scattering event. The probability of light scattering through an angle θ after n scattering events is given by a multiple-scattered phase function, a concept used by Tessendorf and Wasdon [131] to simulate multiple scattering in clouds, and recently applied by Premoze *et al.* [108] in the rendering of objects with subsurface scattering.

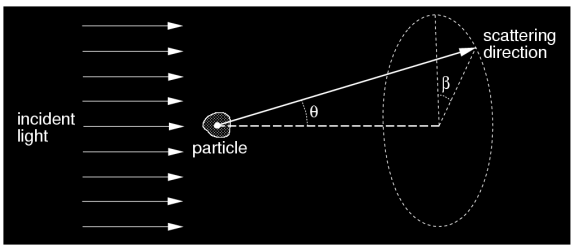

Figure 3: Sketch describing the scattering angles associated with a phase function $\phi(\theta, \beta)$.

In astrophysics, a phase function is treated as probability distribution, and its normalization requires that the integral over all angles to be equal to the unity:

$$\int_{4\pi} \Gamma(\theta, \beta)\ d\omega = 1 \tag{6}$$

The average cosine of the phase function, or asymmetry factor (g), is used to describe the degree of asymmetry of the phase function. It can be defined as:

$$g = \int_{4\pi} \Gamma(\theta, \beta) \cos\theta\ d\omega \tag{7}$$

The simplest phase function is the symmetric one ($g = 0$):

$$\Gamma(\theta, \beta) = \frac{1}{4\pi} \tag{8}$$

The name "phase function" has no relation to the phase of the electromagnetic wave (light). It has its origins in astronomy, where it refers to lunar phases [60]. Coincidentally, one of the most commonly used phase functions in tissue optics, namely the Henyey-Greenstein Phase Function (or simply HGPF), was designed aiming at astrophysical applications [57].

The HGPF was presented by Henyey and Greenstein to approximate Mie scattering in their study of diffuse radiation in galaxies [57]. It is important to note, however, that a theoretical derivation for this phase function was not provided by Henyey and Greenstein [57]. It is defined as:

$$\Gamma_{HG}(g, \theta) = \frac{1 - g^2}{(1 + g^2 - 2g\cos\theta)^{\frac{3}{2}}} \tag{9}$$

The HGPF is actually a function of *three* parameters: g, θ and β. It just happens that an azimuthal symmetry of the phase function is assumed, *i.e.*, the function is constant with respect to β. By varying the parameter g in the range $-1 \leq g \leq 1$, it is possible to characterize HGPFs ranging from a completely backward-throwing to a completely forward-throwing form (Figure 4).

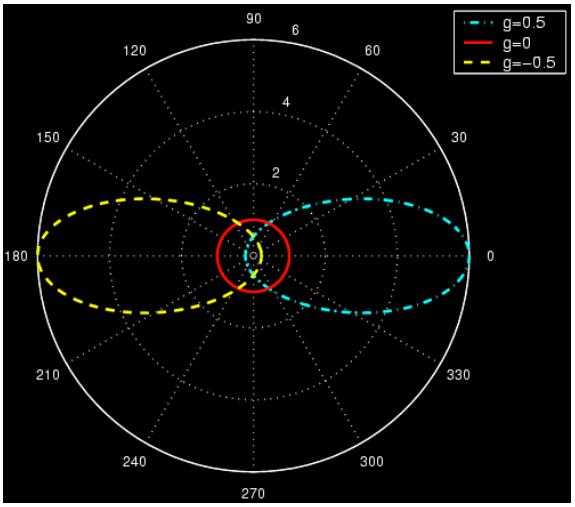

Figure 4: Scattering diagrams illustrating different scattering profiles provided by the HGPF.

The HGPF as defined in Equation 9 cannot, however, be used to describe simultaneous forward and backward lobes which are typical in many cases of Mie scattering as well as Rayleigh scattering [155]. For

this reason, astrophysicists proposed variations based on the superposition of two HGPFs [70, 140, 155]:

$$\Gamma(g_1, g_2, \theta, u) = u\Gamma_{HG}(g_1, \theta) + (1-u)\Gamma_{HG}(g_2, \theta) \quad (10)$$

where $\Gamma(g_1, \theta)$ and $\Gamma(g_2, \theta)$ each are of the form given by Equation 9, and u is a suitably chosen uniformly distributed random number on the interval $[0, 1]$. Figure 5 illustrates three scattering profiles provided by the two-term HGPF.

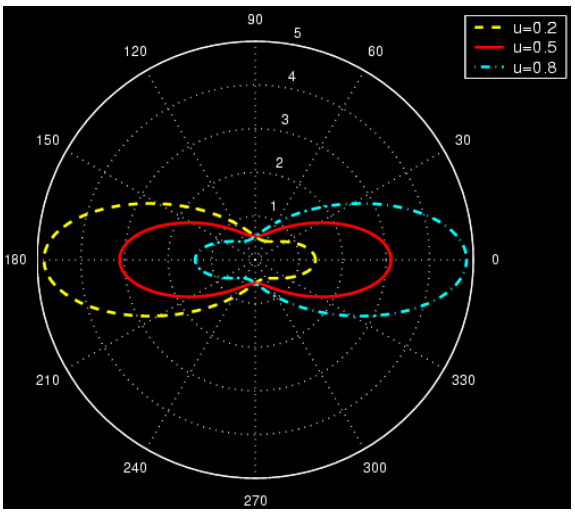

Figure 5: Scattering diagrams illustrating different scattering profiles provided by the two-term HGPF with different asymmetry factors: $g_1 = 0.5$ and $g_2 = -0.5$.

The asymmetry factor is oftentimes called anisotropy factor. We employ the former term throughout this tutorial since we consider the use of the term "anisotropy" inappropriate. Recall that the function has no dependency on the azimuthal angle. Furthermore, there is no direct relationship between this parameter and a macroscopic anisotropic behavior of a given material, *i.e.*, a dependence on both the polar and the azimuthal angles measured from the material's normal and used to define the direction of incidence of the incoming light.

2.4. Measurement of Appearance

The group of measurements necessary to characterize both the color and surface finish of a material is called its *measurement of appearance* [59]. These measurements involve the spectral and the spatial energy distribution of propagated light.

The variations in the spectral distribution of the propagated light affect appearance characteristics such as hue, lightness and saturation [59]. Hue is the attribute of color perception by means of which an object is judged to be red, yellow, green, blue, purple and so forth. Lightness is the attribute by which white objects are distinguished from gray objects and light from dark colored objects. Finally, saturation is the attribute that indicates the degree of departure from the gray of the same lightness.

The changes in the spatial distribution of the propagated light affect appearance characteristics such as gloss, reflection haze, transmission haze, luster and translucency. The reflection haze corresponds to the scattering of reflected light in directions near that of specular reflection by a specimen having a glossy surface [59]. The transmission haze corresponds to the scattering of light within or at the surface of a nearly clear specimen, which is responsible for cloudy appearance seen by transmission [59]. The luster, or contrast gloss, as described by Hunter and Harold [59], corresponds to the gloss associated with contrasts of bright and less bright adjacent areas of the surface of an object. Luster increases with increased ratio between light reflected in the specular direction and that reflected in those diffuse directions which are adjacent to the specular direction. Finally, the translucency property of a material corresponds to incoherent transmission, *i.e.*, a significant portion of the transmitted light undergoes scattering [59].

2.5. Measuring Spectral Distribution of Propagated Light

The spectral energy distribution of the propagated light is usually measured in terms of reflectance and transmittance. Reflectance corresponds to the fraction of light at wavelength λ incident from a direction ψ_i at a point x that is neither absorbed into nor transmitted through a given surface, and it can be represented by $\rho(x, \psi_i, \lambda)$. For the sake of representation simplicity, the dependence on x and ψ_i is usually omitted in the formulas. Alternatively, the reflectance can be defined as the ratio of the reflected flux, Φ_r, to the incident flux, Φ_i, (or the spectral power distribution of the reflected light):

$$\rho(\lambda) = \frac{\Phi_r(\lambda)}{\Phi_i(\lambda)} \quad (11)$$

Similarly, the fraction of light transmitted through the surface is called the transmittance, $\tau(\lambda)$. It represents the ratio of the transmitted flux, Φ_t to the incident flux (or the spectral power distribution of the transmitted light):

$$\tau(\lambda) = \frac{\Phi_t(\lambda)}{\Phi_i(\lambda)} \quad (12)$$

The light that is neither reflected nor transmitted

by the surface is absorbed. The parameter that describes the amount of absorbed light is absorptance [4]. Due to energy conservation, the sum of the reflectance, transmittance and absorptance is one.

For some applications it is more convenient to work with a reflectance factor, $R(\lambda)$, instead of reflectance. It represents the ratio of the reflected flux from a surface to the flux that would have been reflected by a perfectly diffuse surface, Φ_{pd}, in the same circumstances:

$$R(\lambda) = \frac{\Phi_r(\lambda)}{\Phi_{pd}(\lambda)} \tag{13}$$

The transmittance of a homogeneous material, after correction for surface losses, varies in accordance with Bouguer's law (Figure 6), also called Lambert's law of absorption [80]. This law states that the loss due to the process of absorption is proportional to the power of the light incident on the medium, to the thickness of the medium (or the distance traveled by the light in the medium) and to a constant of proportionality called absorptivity [90], which can be represented by specific the absorption coefficient (s.a.c.) of the medium (Section 2.2.3). A complete derivation of this law is presented by Meyer-Arendt [90]. It is usually written as follows:

$$\tau(\lambda) = \frac{\Phi_t(\lambda)}{\Phi_i(\lambda)} = e^{-\zeta(\lambda)\ h} \tag{14}$$

where:

$\zeta(\lambda)$	=	specific absorption coefficient of the medium at λ,
h	=	thickness of the medium,
e	=	Euler's number.

Another law called Beer's law [79] states that for a dye solution (Section 2.2.3), the absorption coefficient of the solution is directly proportional to its concentration. Combining Beer's law with Bouguer's law [80] for samples of thickness h and concentration c results in the following expression for the transmittance of a homogeneous material:

$$\tau(\lambda) = e^{-\zeta(\lambda)\ c\ h} \tag{15}$$

Sometimes it is more convenient to specify the absorption of luminous energy by a medium by means of the extinction coefficient [79, 99], ϵ, which can be expressed as:

$$\epsilon(\lambda) = \frac{\zeta(\lambda)\lambda}{4\pi} \tag{16}$$

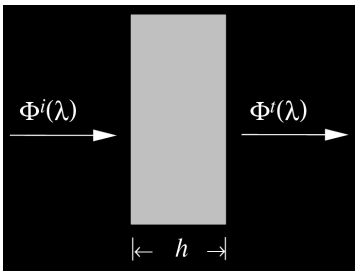

Figure 6: *Loss of light at wavelength λ in a medium of thickness h.*

2.6. Measuring the Spatial Distribution of Propagated Light

The spatial patterns of light distribution [94] can be represented by the *bidirectional scattering-surface distribution function* (BSSDF), or its components, namely the *bidirectional scattering-surface reflectance-distribution function* (BSSRDF) and the *bidirectional scattering-surface transmittance-distribution function* (BSSTDF) [94]. However, as appropriately mentioned by Glassner [50], the BSSDF is a difficult function to measure, store and compute with due its dependency on four parameters: the incidence and outgoing directions, the wavelength and the position on the surface. For this reason, sometimes it is more practical to make simplifying assumptions about the material in order to obtain a more tractable function. For example, if one assumes that a given material's properties are the same everywhere, the position parameter becomes irrelevant [50]. In this case, one can work with simpler function, namely the *bidirectional surface-scattering distribution function* (BSSDF, or simply BDF [50]), which can also be decomposed into two components: the *bidirectional reflectance distribution function* (BRDF) and the *bidirectional transmittance distribution function* (BTDF).

The BDF, f, can be expressed in terms of the ratio between the radiance propagated at a surface in the direction ψ and the radiant energy (per unit of area and per unit of time) incident from a direction ψ_i at the surface:

$$f(\psi_i, \psi, \lambda) = \frac{dL(\psi, \lambda)}{L_i(\psi_i, \lambda)\ d\vec{\omega_i}\ cos\theta_i} \tag{17}$$

where:

$dL(\psi, \lambda)$	=	radiance propagated in a direction ψ,
$L_i(\psi_i, \lambda)$	=	incident radiance in a direction ψ_i,
θ_i	=	angle between the surface normal and the direction ψ_i,
$d\vec{\omega_i}$	=	differential solid angle at which L_i arrives at the surface.

Sometimes, when energy transport or energy balance is of concern as opposed to lighting at a point, it is more convenient to work with the radiant power (radiant flux) [4] than with the radiance [119]. Under these circumstances, it is more natural to describe the surface reflection and transmission properties in terms of the probability distribution of the reflected and transmitted light. This term is called the *scattering probability function* (SPF) [118, 119]. It describes the amount of energy scattered in each direction ψ, at a surface and at wavelength λ as:

$$s(\psi_i, \psi, \lambda) = \frac{dI(\psi, \lambda)}{\rho(\psi_i, \lambda) d\Phi(\psi_i, \lambda)} \qquad (18)$$

where:

$dI(\psi, \lambda)$ a	=	radiant intensity reflected in direction ψ,
$\rho(\psi_i, \lambda)$	=	reflectance of the surface with respect to the incident direction ψ_i,
$d\Phi(\psi_i, \lambda)$	=	radiant power (flux) incident in a direction ψ_i.

The term $\rho(\psi_i, \lambda)$ appears in the numerator when we are dealing with reflection of light. It scales the function to a valid *probability density function* (PDF) over the solid angle through which the reflected light leaves the surface [118, 119]. In the case of transmission of light, a similar expression is used, in which $\rho(\psi_i, \lambda)$ is replaced by $\tau(\psi_i, \lambda)$.

3. Biological Issues

Skin is a multilayered and inhomogeneous organ. In this section, we outline the biological characteristics of its main constituents, and how they affect the propagation and absorption of light.

3.1. Factors Affecting Light Interaction with Skin Tissues

In order to simulate the mechanisms of photon transport and absorption within skin tissues, it is necessary to account for the biological and structural characteristics of these tissues and their constituents. Factors like the internal arrangement of the tissues and their thickness as well as the concentration and distribution of pigments have a direct effect on the skin appearance as illustrated in Figure 7. For this reason, these factors are examined in more detail in the next sections. It also worth noting that surface features, such as the presence of hair, oil and sweat, may also affect skin appearance.

Figure 7: Photographs showing the different appearance of the inner and outer surfaces of an individual's hand.

3.2. Skin: Structural Characteristics and Spectral Properties

The first and outermost section of human skin is the stratum corneum, which is a stratified structure approximately 0.01-0.02 mm thick [2, 86]. There are skin structural models, however, that consider it part of another tissue, namely the epidermis [138] (Figure 8). The stratum corneum is composed mainly of dead cells, called corneocytes, embedded in a particular lipid matrix [130]. Light absorption is low in this tissue, with the amount of transmitted light being relatively uniform in the visible region of the light spectrum [40].

The epidermis is a 0.027-0.15mm thick structure [2, 32, 86] composed of four layers (stratum basale, stratum spinosum, stratum granulosum and stratum lucidum). The epidermis propagates and absorbs light. The absorption property comes mostly from a natural pigment (or chromophore), melanin. There are two types of melanin, the red/yellow phaeomelanin and a brown/back eumelanin [133]. Their absorption spectra are broad (Figure 9), with higher values for shorter wavelengths. The skin color is mostly associated with eumelanin [133]. The ratio between the concentration of phaeomelanin and eumelanin present in human skin varies from individual to individual, with much overlap between skin types [133]. Recent studies reported values between 0.049 and 0.36 [100]. Melanin is produced by cells called melanocytes occurring in the stratum basale, and it is found in membranous particles called melanosomes. The melanin absorption level depends on how many melanosomes per unit volume are in the epidermis. Typically, the volume fraction of the epidermis occupied by melanosomes varies from 1.3% (lightly pigmented specimens) to 43% (darkly pigmented specimens) [63].

The dermis is a 0.6-3mm thick structure [2, 32, 86] which also propagates and absorbs light. It can be divided into two layers: the papillary dermis and the

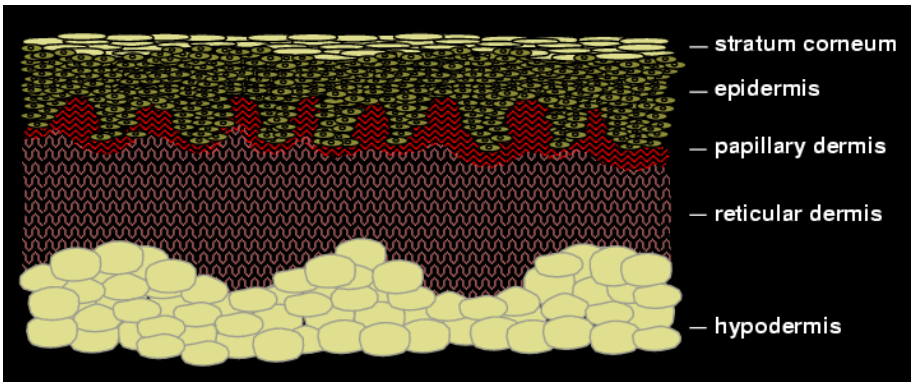

Figure 8: Schematic cross-section of skin tissues and the subcutaneous tissue (hypodermis).

reticular dermis (Figure 8). These layers are primarily composed of dense, irregular connective tissue with nerves and blood vessels (smaller ones in the papillary, and larger ones in the reticular dermis). The volume fraction of blood in tissue can vary, roughly in the 0.2-7% range [43, 63]. The fluence rate of blood decreases as we get deeper into the skin, following an almost linear pattern in the dermis [145]. In the blood cells we find another natural chromophore, hemoglobin, which absorbs light and gives blood its reddish color. Normally, the hemoglobin concentration in whole blood is between 134 and $173 g/L$ [156]. In the arteries, 90-95% of hemoglobin is oxygenated, and in the veins, more than 47% of the hemoglobin is oxygenated [3]. These two types of hemoglobin, namely oxygenated and deoxygenated hemoglobin, have slightly different absorption spectra (Figure 9). Two other blood borne pigments are found in the dermis, bilirubin and β-carotene, which contribute to the yellowish or olive tint of human skin (Figure 9). We remark that β-carotene may be also found in the epidermis and stratum corneum [1, 77].

The hypodermis is an adipose tissue characterized by a negligible absorption of light in the visible region of the spectrum [43]. It is usually not considered part of the skin, and its size varies considerably throughout the body. It can be up to $3cm$ thick in the abdomen and absent in the eye lids. The hypodermis presents significant deposits of white fat, whose cells are grouped together forming clusters. Due to the presence of these white fat deposits, most of the visible light that reaches this tissue is reflected back to the upper layers [32].

3.3. Scattering Profile

The scattering profile of human skin has two main components: surface and subsurface scattering. Surface scattering follows Fresnel equations [128], and it is affected by the presence of folds in the stratum corneum. The aspect ratio of these mesostructures depends on biological factors such as aging and hydration [130, 132]. Approximately 5-7% of the light incident (over the entire spectrum) on the stratum corneum is reflected back to the environment [138]. The remaining portion is transmitted to the internal tissues. Besides the reflective-refractive scattering caused by the reflection and refraction of light at cellular boundaries, two other types of scattering occur within the skin layers: Mie and Rayleigh scattering [63].

The stratum corneum and the epidermis are characterized as forward scattering media [19]. In the former this behavior is due to the alignment of the fibers, while in the later it is due to Mie scattering caused by particles that are approximately the same size of the wavelength of light (*e.g.*, cell organelles). Furthermore, the level of forward scattering for these tissues is wavelength dependent as demonstrated by the goniometric measurements (BTDF) performed by Bruls and van der Leun [19] for both the stratum corneum and the epidermis (Figure 10). Considering, for example, the fraction of energy transmitted within an angle of 22.5° of the sample's normal at 546nm, it corresponded approximately to 83% and 59% for stratum corneum and epidermis samples respectively. When these vales are compared to the value computed for a diffusively scattering sample (14.6% within 22.5° from the normal), they clearly illustrate the forwardly scattering orientation of these tissues.

In the dermis, collagen fibers (approximately $2.8\mu m$ in diameter and cylindrical [63]) are responsible for Mie scattering, while smaller scale collagen fibers and other micro-structures are responsible for Rayleigh scattering [63]. Light gets scattered multiple times inside the dermis before it is either propagated to an-

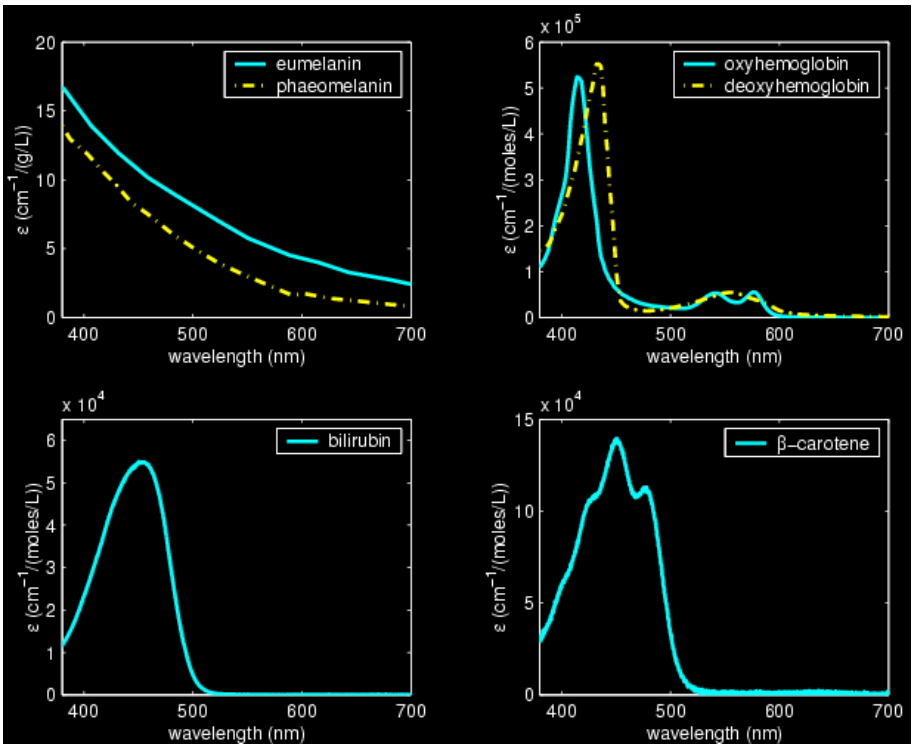

Figure 9: Molar extinction coefficient curves for pigments present in skin tissues. Courtesy of S. Prahl and the Oregon Medical Laser Center. Absorption spectra are obtained by multiplying each curve by the pigment's molecular weight and concentration.

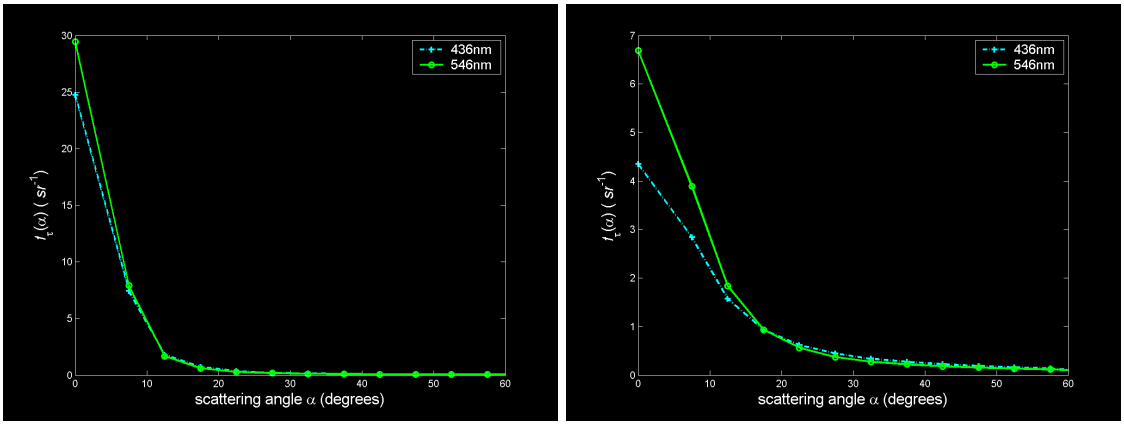

Figure 10: Graphs showing the BTDF measurements performed by Bruls and van der Leun [19] for stratum corneum (left) and epidermis (right) samples.

other layer or absorbed. This means that the spatial distribution of the light scattered within the dermis quickly becomes diffuse [2], as shown in Figure 11. In fact, Jacques *et al.*, [64] showed through goniometric measurements that backscattered light from the dermis is diffuse. While Mie scattering produces variations on both ends of the visible region of the light spectrum, Rayleigh scattering, being inversely proportional to the wavelength of light ($\approx \lambda^{-4}$), produces

larger variations on the low end of the light spectrum [63].

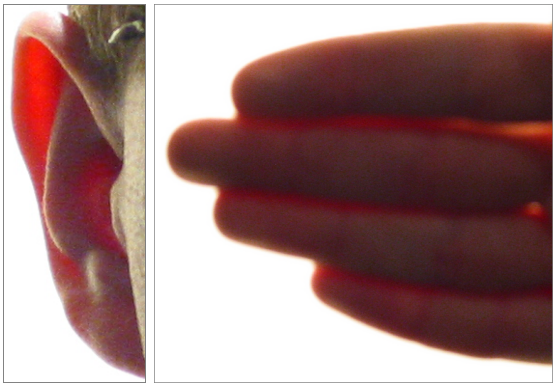

Figure 11: Photographs illustrating the diffuse pattern of transilluminated light emerging from skin tissues.

3.4. Interactions with Invisible Light

Although in computer graphics we usually deal with visible light, one cannot overlook the role played by invisible light (ultraviolet and infrared) since they may cause very noticeable visible effects on the human skin. Furthermore, emerging medical visualization technologies, such as infrared thermography[‡‡], are based on biophysical processes triggered by invisible radiation.

Ultraviolet light can induce processes such as erythema (an abnormal redness of the skin caused by a dilation of the blood vessels followed by an increase in the volume fraction of blood in the dermal layers), melanogenesis (melanin production) and photoaging (discoloration and wrinkle formation) [71, 73, 144, 101]. According to the CIE (*Commission Internationale de L'Eclairage*), ultraviolet radiation can be divided into three regions [12]: UV-A (ranging from 315nm to 380nm), UV-B (ranging from 280nm to 315nm) and UV-C (ranging from 100nm to 280nm). The UV-C is mostly absorbed by the ozone layers in the atmosphere. UV-B penetrates deeper than UV-C in skin layers, and it may increase the melanogenesis after a certain period (6-8 hours) that follows the erythema reaction [73]. UV-A penetrates deeper than UV-B, and it can induce epidermal pigmentation immediately with exposure [73]. There are only a few exogenous chemical substances that can absorb UV-A efficiently [126]. Commercial tanning beds emit mostly ultraviolet light in the UV-A range. Although the lack of UV-B in infants and small children may lead to disruption of bone growth and increase the probability of tooth decay [126], overexposure to ultraviolet radiation can induce the formation of melanomas [42] and carcinomas [101]. The former is the most serious form of skin cancer since it presents high metastatic potential and low cure rates [42]. Not surprisingly, a substantial amount of research and resources are applied in the development of effective sunscreens [126].

Heating of tissues in the human body is the principal effect of infrared radiation, and excessive exposure can also induce erythema reactions in the skin. The primary source of infrared radiation is heat or thermal radiation (Section 2.2.1), *i.e.*, the radiation produced by the motion of atoms and molecules in an object. The higher the temperature, the more the atoms and molecules move and the more infrared radiation they produce. Humans, at normal body temperature (around 35° or 308K), radiate most strongly in the infrared. In fact, for infrared radiation the human body is a very good approximation to an ideal blackbody (Figure 12), irrespective of skin pigmentation [115]. This biophysical characteristic of the human body has motivated the increasing application of infrared thermography in medical diagnosis.

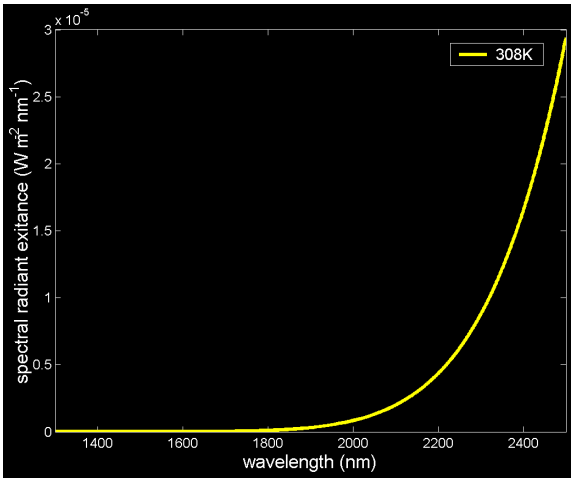

Figure 12: *Spectral energy distribution of a blackbody radiator of* $308K$.

4. Review of Models Used in Biomedical Applications

In this section we provide an overview of relevant simulation approaches and models used in biomedical ap-

[‡‡] Infrared thermography corresponds to the use infrared imaging and measurement devices to "visualize" thermal energy emitted from a material. Medical applications of infrared thermography include the use of skin temperature as an indicator of a subcutaneous pathological process [95].

plications involving tissue optics, and group them according to their similarities. For a comprehensive literature review on this topic, the reader is referred to the texts by Cheong *et al.* [24] and Tuchin [138].

4.1. Scope of Applications

The models of light interaction with human skin developed by the biomedical community are usually designed for the noninvasive measurement of tissue optical properties, and aimed at medical applications such as diagnostic spectroscopy and therapeutic dosimetry. It is worth noting that a substantial portion of the modeling work done in this field is either laser-based or aimed at wavelengths outside the visible region of the light spectrum.

The models used in biomedical applications provide as output the spectral power distribution (reflectance and transmittance) of skin tissues, *i.e.*, spatial (directional) power distribution quantities (BDF) are usually not considered. Once the accuracy of these models is established through comparisons of modeled results against actual measured data, they are employed in inversion procedures [161].

An inversion procedure is a way to derive biochemical and optical properties from *in situ* and noninvasive measurements. The term "inversion" in this context implies a reversal of the actual process of calculating reflection and transmission, *i.e.*, using reflectance and transmittance values as input one can determine absorption and scattering properties of the tissues (Figure 13). Similar approaches are used in colorimetry to determine the relationship between color appearance and the content and distribution of various pigments [136].

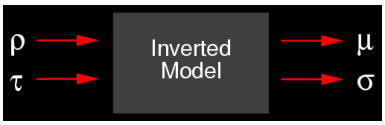

Figure 13: *Sketch illustrating the general idea behind inversion procedures, i.e., a reflectance (ρ) and transmittance (τ) model is inverted and use to determine tissue optical parameters such as attenuation (μ) and albedo (ϱ).*

4.2. Kubelka-Munk Theory Based Models

In the beginning of the century, Kubelka and Munk [76] developed a simple relationship between the scattering and absorption coefficients of paint and its overall reflectance. This relationship is known as the Kubelka-Munk theory (henceforth referred to as K-M theory). Although it was originally developed for paint, it allows a simple quantitative treatment of tissue spectral properties. Incidentally, the term "albedo" (*helligkeit*) was used by Kubelka and Munk [76] to represent the fraction of diffuse light reflected by a matte, plane parallel coating of a given thickness. In the context of this tutorial, however, unless otherwise stated, albedo refers to the definition given in Section 2.3.

The K-M theory applies energy transport equations to describe the radiation transfer in diffuse scattering media using two parameters: the scattering and the absorption coefficients. The K-M theory, as originally stated, is considered to be a two-flux theory since only two types of diffuse radiant flux are involved, namely a diffuse downward flux and a diffuse upward flux. The relations between the fluxes are expressed by two simultaneous linear differential equations [76]. The original K-M theory also assumes that the medium (specimen) presents inhomogeneities which are small compared to its thickness.

The K-M theory based models (henceforth referred to as K-M models), used in biological tissue optics, also called flux models [24], use K-M equations relating tissue optical properties to measured reflectance and transmittance. Although these analytical models allow a rapid determination of optical properties through inversion procedures, their relative simplicity and speed are provided at the expense of accuracy [138], which has been improved by adding more coefficients and/or fluxes to the original two-flux K-M theory.

For example, van Gemert and Star [146] included a phase function, optical depth and the effective albedo in their K-M model. They used a phase function consisting of a combination of a forward peaked and a symmetric scattering to represent the tissue's expected experimental scattering behavior. Tuchin *et al.* [139, 157] used a four-flux model composed of the two diffuse fluxes used in the original K-M theory, and two fluxes represented by collimated laser beams, an incident one and the beam reflected from the bottom boundary of the specimen (Figure 14).

Yoon *et al.* [160, 158] used a seven fluxes model (Figure 15) to obtain a three dimensional representation of the scattered radiation caused by an incident laser beam in a semi-infinite medium (infinite in x and y, but finite in z). They also incorporated a phase function composed of a symmetric term and a HGPF term.

In skin optics, the K-M theory was initially applied to specific skin tissues. Anderson and Parish [2] used a K-M model to compute absorption and scattering coefficients for the dermis tissues. Wan *et al.* [151]

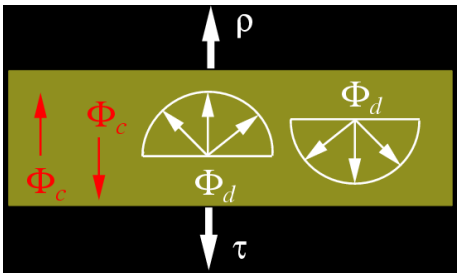

Figure 14: *Sketch illustrating the four fluxes used in the model developed by Tuchin et al. [139, 157], namely two diffuse fluxes (Φ_d) used in the original K-M theory, and two fluxes represented by collimated laser beams (Φ_c).*

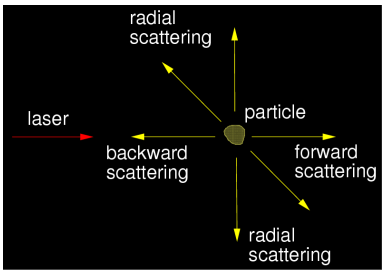

Figure 15: *Sketch illustrating the seven fluxes considered in the model developed by Yoon et al. [160, 158].*

extended this model to compute the absorption and scattering coefficients for the epidermis tissues, taking into account both collimated and diffuse incident irradiance. In both cases [2, 151], the forward scattering in the epidermis was not considered. Diffey [31] proposed a K-M model which added two features to the previous models, namely it takes into account forward and backward scattering and allows changes in the refractive index at the air⟺skin interfaces. Cotton and Claridge [29] proposed a model to determine the color of human skin which applies the K-M equations to the dermis layer. This model takes into account the presence of melanin and blood pigments. Recently, Doi and Tominaga [32] presented a model which considers the skin composed of two layers: epidermis and dermis. They apply the K-M theory to both layers. Their model provides weights for five skin pigments (melanin, carotene, oxy-hemoglobin, deoxy-hemoglobin and bilirubin) as well as the skin surface reflectance. These six parameters are obtained by fitting the estimated reflectance to measured values (Figure 16) using the least squares method [20].

Although recent extensions to the original two-flux theory have improved the accuracy of K-M based models and their applicability to biological tissue optics, they cannot be considered thorough models of optical radiation transfer since they lack a more detailed analysis of the structure and optical properties of the different skin tissues. It is important to note that the development K-M based models for the investigation of tissue optics is not limited to the biomedical field. For example, substantial advances in this area were are also obtained in fields such as remote sensing [10]. However, it seems that there is no exchange of concepts and ideas among these fields. We believe that such cross-fertilization would be beneficial for the advancement of tissue optics research.

4.3. Diffusion Theory Based Models

Photon propagation in optically turbid media, such as skin tissues, can be described using the Boltzmann photon transport equation [60], which requires the optical properties of the medium to be expressed in terms of scattering coefficient, absorption coefficient and phase function. Diffusion theory can be seen as an approximate solution of this equation. It assumes a scattering-dominated light transport, and it combines the scattering and the phase function in one parameter, called reduced scattering coefficient, which is given by:

$$\mu_s' = \mu_s(1-g) \tag{19}$$

Models based on the diffusion approximation [147] or combined with other approaches, such as the K-M theory [146, 145] or Monte Carlo methods [152], have been used in biomedical investigations involving light propagation in turbid media including skin tissue. For example, Schmidt *et al.* [113] presented a multilayer model which describes the propagation of a photon flux in the epidermal, dermal and subcutaneous tissue layers of skin, and assumes that the specimen is illuminated by a collimated, finite aperture light source. The predictive ability of the model proposed by Schmidt *et al.* [113] is limited by the practical difficulty of obtaining accurate values of scattering and absorption coefficients for the different skin tissues.

Farrell and Patterson [41] proposed a model based on the diffusion theory to be used in the noninvasive determination of the absorption and scattering properties of mammalian tissues. Their model incorporates a photon dipole source approximation in order to satisfy the tissue boundary conditions (Figure 17), namely light being remitted from a tissue from point different from the incidence point and the presence of thin layers of dirt, blood or other fluids on the surface of the tissue under investigation.

This dipole approximation was originally used by

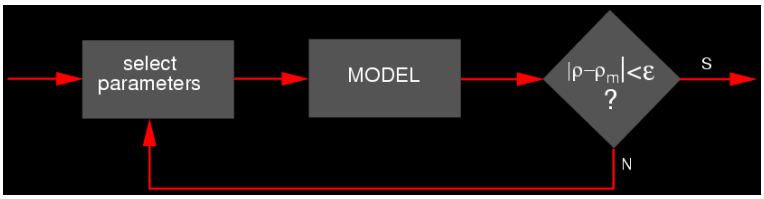

Figure 16: *Flowchart illustrating the iterative process used by Doi and Tominaga [32] to obtain skin parameters by comparing the difference between the modeled reflectance, ρ, and the measured reflectance, ρ_m, with a error threshold, ϵ.*

Freterd and Longini [47] and Hirko *et al.* [58], and further developed by Eason *et al.* [39]. Farrell and Patterson [41] considered two additional boundary conditions: a refractive index mismatch interface (tissue$\Longleftrightarrow$air) and a refractive index matched surface. The predictions of their model were compared with skin optical properties obtained using Monte Carlo simulations, and the results presented a poor agreement.

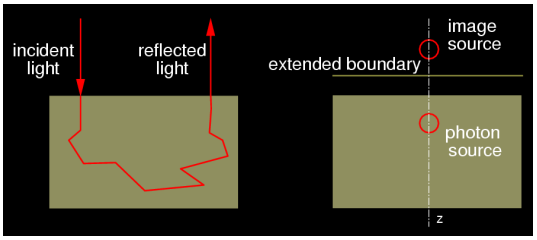

Figure 17: *Sketch illustrating the boundary conditions taken into account by the dipole approximation. Left: light being remitted from a tissue from point different from the incidence point. Right: extended boundary to account for the presence of thin layers of dirt, blood or other fluids on the surface of the tissue under investigation.*

Recently, Doornbos *et al.* [35] proposed a hybrid method based on the diffusion theory for measuring optical properties and deriving chromophore concentrations from diffuse reflection measurements at the surface of a turbid media. Their method consists in measuring tissue reflectance and using the diffusion approximation to obtain the optical properties from the values measured in the wavelength domain for which this approximation holds. Doornbos *et al.* [35] consider the $650 - 1030nm$ domain in their experiments. Initially, they approximate the wavelength dependency of the reduce scattering coefficient using a Mie function, and use these values to recalculate the tissue absorption and scattering coefficients with a higher accuracy. These coefficients are used to determined the concentration of the absorbers, namely water, oxyhemoglobin and deoxyhemoglobin. Although this hybrid method has provided results in the physiological range [35], the accuracy of the modeled *in vivo* concentrations cannot be properly assessed due to the difficulties involved in the direct and simultaneous measurement of these concentrations in living tissue.

Models based on the diffusion theory are amenable to analytic manipulation, place minor constraints on the type of sample and are relative easy to use [105]. The diffusion theory, however, can be applied only when scattering events are more probable than absorption events. This is usually the case for mammalian tissues in the red and near infrared regions of the light spectrum[44]. Not surprisingly, diffusion models have been used in medical applications involving red lasers [147, 159]. When the absorption coefficient of a turbid medium is not significantly smaller than the scattering coefficient, the diffusion theory provides a poor approximation for the photon transport equation [127, 112, 159].

4.4. Radiative Transport Models

The K-M and diffusion theories mentioned in the previous sections can be seen as special cases of radiative transfer phenomena. When non-stochastic accurate solutions of the radiative transport equation in biological tissues are required, more robust methods need to be used, *e.g.*, the successive scattering technique, Ambartsumian's method, the discrete ordinate method, Chandrasekhar's X and Y functions and the adding-doubling method [103]. Their applicability, however, is usually limited to simple conditions and slab geometries[§§]. A comprehensive review of these methods is beyond the scope of this tutorial, and the interested reader is referred to the texts by van de Hulst [141] and Prahl [103]. It is worth noting, however, that the adding-doubling method has several advantages with

[§§] In the tissue optics context, a "slab" refers to an infinite plane parallel layer of finite thickness [103].

respect to the other techniques. It permits asymmetric scattering, arbitrarily thick samples, Fresnel boundary conditions, and relatively fast computation [103].

The adding method requires that the reflectance and transmittance of two slabs be known. They are used to compute the reflectance and transmittance of another slab comprised of these two individual slabs. Once the transmittance and reflectance for a thin slab are known, the reflectance and transmittance for a target slab can be computed by doubling the thickness of the thin slab until it matches the thickness of the target slab (Figure 18). In the original definition of this doubling method, it is assumed that both slabs are identical [141]. Later on, this method was extended to include the addition of two non-identical slabs [103].

Prahl *et al.* [105] applied an inverse adding-doubling method (IAD: "inverse" implying its use as an inversion procedure) to determine the scattering, absorption coefficient and the asymmetry factor of biological tissues. The IAD is an iterative method which consists of guessing a set of optical properties, calculating the reflectance and transmittance using adding-doubling method, comparing the calculated values with the measured reflectance and transmittance, and repeating the process until a match is obtained. This method may be used when the propagation of light through the specimen can be described by the one-dimensional radiative transport equation. The accuracy of this method, however, depends on the criteria applied to define a "sufficiently thin slab" [103]. There are also restrictions on the sample geometry, *i.e.*, it must be an uniformly illuminated and homogeneous slab [105].

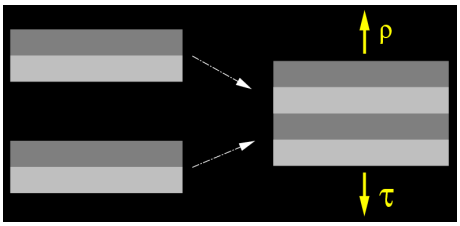

Figure 18: *Sketch illustrating the application of the adding-doubling method to compute the reflectance and transmittance of a target tissue slab.*

4.5. Monte Carlo Based Models

The Monte Carlo method was originally proposed by Metropolis and Ulam [89] as an statistical approach to the study of integro-differential equations that occur in various branches of natural sciences. However, instead of dealing with multiple integrations, radiative transfer processes are stochastically simulated as chains of events. In the case of processes involving light interaction with matter, this approach consists in keeping track of photon histories as they are scattered and absorbed in a given medium.

Monte Carlo models have been extensively used to simulate biological tissue optics [138] since they can provide a flexible, and yet rigorous approach to this problem [152]. These models can be easily implemented, and they are sufficiently flexible to allow the simulation of complex tissues. Theoretically, Monte Carlo solutions can be obtained for any desired accuracy [103]. In practice, the accuracy of Monte Carlo simulations is bounded by the accuracy of the input parameters and the use of proper representations for the mechanisms of scattering and absorption of photons. The core of Monte Carlo models of light transport in turbid media is represented by the scattering profile of the particles, which can be described by a phase function (Section 2.3).

In 1984, Bruls and van der Leun [19] suggested their measurements of the scattering profile of stratum corneum and epidermis tissues (Section 3.3) could be approximated by single particle phase functions, the HGPF. Jacques *et al.* [64] followed Bruls and van der Leun's suggestion, and tried to approximate the measured scattering profile of another skin tissue, namely dermis, using the HGPF with an asymmetry factor $g = 0.81$. Yoon *et al.* [160] used similar asymmetry factor (g) values for human aorta. The experiments on dermis and aorta tissues were aimed at specific medical applications and conducted with a HeNe laser (632.8nm). Motivated by these works, Prahl [103] proposed a Monte Carlo based algorithm to model light transport in tissue during laser irradiation. Although this Monte Carlo based approach was used before to study light propagation in tissue [154], Prahl's algorithmic formulation, to the best of our knowledge, was the first proposed to use the HGPF to compute the scattering of photons in organic tissues. In order to compute the trajectories of the scattered photons, Prahl [103] used a warping function provided by Witt [155], which was derived from the HGPF by setting:

$$\xi_1 = 2\pi \int_{-1}^{\cos\theta} \Gamma(cos\theta', g) d\cos\theta', \qquad (20)$$

and finding upon integration that

$$\cos\theta = \frac{1}{2g}\left\{1 + g^2 - \left[\frac{1-g^2}{1-g+2g\xi_1}\right]^2\right\}, \qquad (21)$$

where ξ_1 is an uniformly distributed random number on the interval $[0, 1]$. For symmetric scattering (g=0) the expression $\cos\theta = 2\xi_1 - 1$ should be used [104]. Since an azimuthal symmetry of the phase function is assumed, the azimuthal angle can be generated using

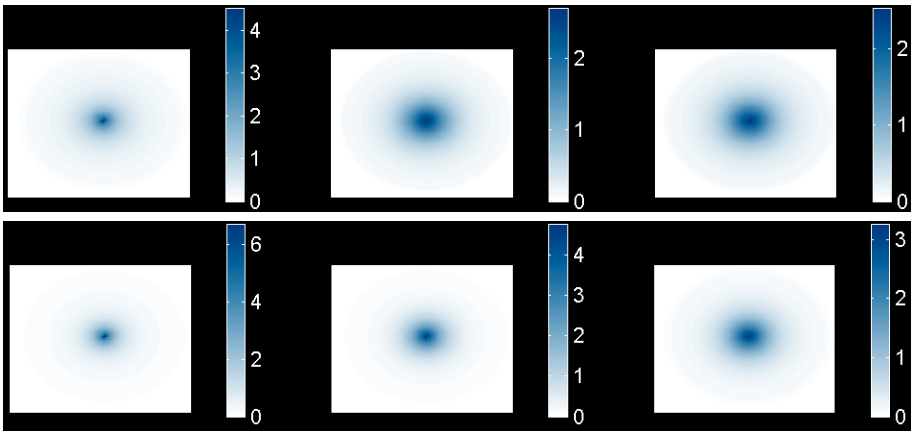

Figure 19: *Comparison of measured and modeled scattering diagrams (orthographic projections) for an epidermis sample considering light incident at 436nm (top row) and 546nm (bottom row). Left column: using measured data [19]. Middle column: using the HGPF with g=0.761 (RMS error metric [8]). Right column: using the HGPF with g=0.748 (least squares method [145]).*

$\beta = 2\pi\xi_2$, where ξ_2 is a random number uniformly distributed on the interval $[0, 1]$.

In 1989, van Gemert *et al.* [145] attempted to fit the HGPF to the goniometric measurements of Bruls and van der Leun [19], and used the least squares method to determine suitable values for g (Figure 19). Recently, Baranoski *et al.* [8] have shown that other techniques, such as the RMS error metric (Figure 19), may be used to determine values for g that can provide a closer quantitative agreement to the data measured by Bruls and van der Leun [19]. It is important to recall, however that the asymmetry factor g has no direct connection with the underlying biophysical phenomena.

Even though the original goal behind the the use of the HGPF and its variations in tissue optics was just the fitting of data measured at specific wavelengths, their application has been extended to different organic materials despite the lack of supporting measured data and the fact that their parameters have no biological meaning. Clearly, such generalized use of these functions may affect the accuracy of the simulations as demonstrated biomedical investigations [36, 91, 7], and, more recently, in computer graphics investigations [8].

To the best of our knowledge, the Monte Carlo models used in biomedicine [25, 86, 87, 104, 117, 122], colorimetry [136] and pattern recognition [92] provide only reflectance and transmittance readings for skin samples, *i.e.*, BRDF and BTDF quantities for the whole skin are not computed. We remark that these models are mostly aimed at laser applications, and comparisons of modeled reflectance and transmittance values with actual measured values are scarce.

5. Multiple-Layer Scattering Model

In 1993, Hanrahan and Krueger [54] proposed a model to simulate subsurface reflection and transmission from layered surfaces, [50]. This intuitive idea of a layered surface model has appeared before in fields such as remote sensing [61, 10] and tissue optics (Section 4). The model proposed by Hanrahan and Krueger, henceforth referred as the H-K model, to the best of our knowledge, was the first computer graphics scattering model to incorporate tissue optics concepts and techniques, and to consider subsurface reflection and transmission from layered natural materials. It can be used to simulate the scattering profile of layered materials appearing in nature, such as biological tissues (*e.g.*, skin and leaves) or inorganic materials (*e.g.*, snow and sand). In this tutorial, however, it is examined in the context of the rendering of human skin which was modeled by Hanrahan and Krueger as two layers, epidermis and dermis.

5.1. Overview

Hanrahan and Krueger [54] assumed planar surfaces, and used Fresnel coefficients to find how much light will pass through the outermost surface of the coating. The model then evaluates the scattering and absorption within each layer, including the reflection and transmission effects at each internal boundary. The BRDF and BTDF are described by a combination of the reflection function on the outer surface

and the internal subsurface scattering handled by a Monte Carlo algorithm which was originally proposed by Prahl [103, 104] to investigate laser irradiation in tissue (Section 4.5).

In the H-K model, it is assumed that if a material is a mixture of several materials, then the mixture can be considered to be an uniform and homogeneous combination whose properties are given by a sum of the descriptors of the components weighted by percentages. The material descriptors include the index of refraction, the absorption cross section, the scattering cross section, the depth (or thickness) and a phase function (the HGPF). The absorption and scattering cross sections used by Hanrahan and Krueger correspond in fact to the volumetric absorption and scattering coefficients respectively (Section 2.3). In this tutorial, for the sake of consistency with the tissue optics literature, we use the terms absorption coefficient and scattering coefficient instead of the terms absorption cross section and scattering cross section used by Hanrahan and Krueger [54].

5.2. Scattering Simulation

The H-K multiple-layer model assumes that the reflected radiance from a surface has two components (Figure 20). One arises due to surface reflectance (L_{rs}) and the other due to subsurface volume scattering (L_{rv}). It also assumes that the transmitted radiance has two components (Figure 20). One, called *reduced intensity*, represents the amount of light transmitted through the layer without scattering inside the layers, but accounting for absorption (L_{ri}), and the other is due to scattering in the volume (L_{tv}). Similarly, the BRDF and BTDF also have two components, and the relative contributions of the surface and subsurface terms are modulated by the Fresnel coefficients. Clearly, the variations on the polar angle of incidence, given by θ_i, will affect the value of these coefficients, which in turn will affect the magnitude of BRDF and BTDF components. Incidentally, since there is no dependency on the azimuthal angle of incidence, the H-K model can be classified as an isotropic model.

5.2.1. Surface Reflection

As indicated by Hanrahan and Krueger [54], surface reflection is handled using the Torrance and Sparrow model [134]. In this model, reflected energy is attenuated due to orientations of surface microfacets according to a multiplicative exponential factor $e^{-\varsigma^2/m^2}$, where the angle α corresponds to the inclination of the microfacets with respect to the normal of the mean surface, and the parameter m can be seen as their root mean square (RMS) slope. It should be cautioned that the value of the parameter m should not be very large, otherwise the results may become quite physically implausible. According to experiments performed by Torrance and Sparrow [134], the value of this parameter should range from 5 to 100 for inorganic materials such as ground glass surfaces. Other issues related to the use of this model in conjunction with the H-K model are addressed in Section 5.3.

5.2.2. Subsurface Reflection and Transmission

Hanrahan and Krueger [54] examined the application of first-order approximations for the analytical solution of the integral transport equation assuming only a single scattering event [22]. The first order solution for L_{tv} is obtained by replacing L_{ri} in the integral equation [22], and the first order solution for L_{rv} is obtained by applying Seeliger's formulation for diffuse reflection [¶¶]. These first order solutions are used in the first step of a refinement approach which consists in substituting the ith-order solutions in the integral equation and solving to get the $(i+1)th$-order solutions.

As stated by Hanrahan and Krueger, this analytical refinement approach "quickly becomes intractable". Thus, alternatively, the H-K model applies an algorithmic approach for computing light transport in a layered semi-finite turbid media with different albedos (γ). More precisely, the subsurface scattering is simulated using a Monte Carlo algorithm previously applied in the biomedical field (Section 4.5). Since the H-K model [54] represents the first biologically motivated effort in computer graphics to account for subsurface reflection and transmission from layered natural materials, its algorithmic formulation is examined in some detail as follows:

1. As a ray enters the layer at the origin, initialize point $\vec{o}$ to the origin, and the direction $\vec{s}$ to the direction at which the ray enters the layer. Set the ray weight to $w = 1$.
2. Repeat the following steps until the ray weight drops below a given threshold or the ray exits the layer.

   2.1 Estimate the distance to the next iteration using

[¶¶] Seeliger [116] attempted to explain experimental deviations from Lambert's Law by relating the scattering to the structure of a particular material under consideration. He quantitatively used a hypothesis originally proposed by Bouguer [18] which consists in assuming a surface to be composed of countless small elementary mirrors disposed at all possible angles [15, 11]

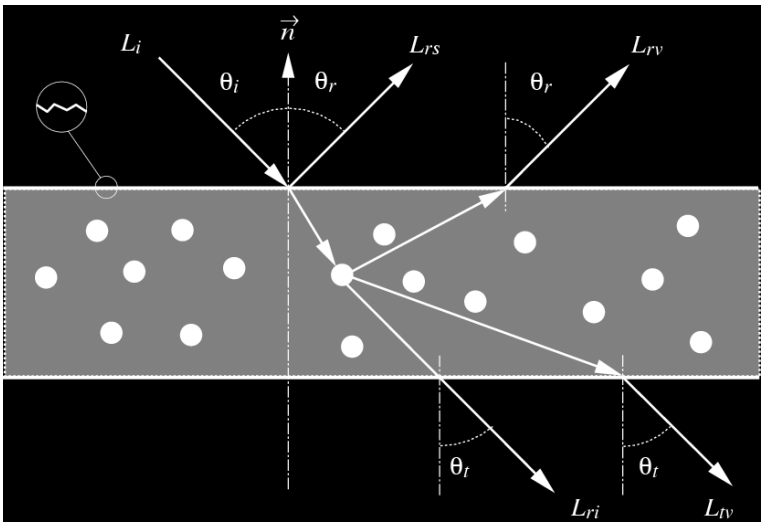

Figure 20: *Sketch of the scattering geometry used in the H-K multiple-layer model.*

the following formula:

$$d = -\frac{log\xi_1}{\mu_s + \mu_a}$$

where ξ_1 corresponds to an uniformly distributed random number $\in [0, 1]$.

2.2 Compute the new position, *i.e.*, $\vec{o} \leftarrow \vec{o} + d\vec{s}$.

2.3 Set the ray weight to $w \leftarrow w\ \gamma$.

2.4 Compute the cosine of the scattering angle using Equation 21.

2.5 Perturb the ray direction using

$$\vec{s} = \vec{s}\ cos\theta + \vec{t}\ sin\theta$$

where:

$$\vec{t} = \begin{pmatrix} (\vec{s}.x\ cos\beta\ cos\phi - \vec{s}.y\ sin\beta)/sin\phi \\ (\vec{s}.y\ cos\beta\ cos\phi + \vec{s}.x\ sin\beta)/sin\phi \\ sin\theta \end{pmatrix}$$

$$\beta = 2\pi\xi_2$$

where ξ_2 corresponds to an uniformly distributed random number $\in [0, 1]$.

$$cos\phi = \vec{s}.z$$

$$sin\phi = \sqrt{1 - (\vec{s}.z)^2}$$

3. Divide the sphere surrounding the materials into regions of equal solid angle increments. These regions are considered to be bins receiving emitted rays. When a ray exits the material, add the weight of the ray to the weight of the bin that receives it.

5.3. Implementation Issues

The H-K model was originally implemented as an extension to a standard ray tracer developed using *Rayshade* [72], a public domain software for rendering applications written in *C*, *lex* and *yacc*.

The skin tissues, namely epidermis and dermis, and their constituents are considered as dielectrics, and Hanrahan and Krueger [54] assign to them indices of refraction between 1.37 and 1.5. Although Hanrahan and Kruger do not provide a direct reference to the source from which the values for the absorption and scattering coefficients and asymmetry factors used in their experiments were obtained, it was implied that they could be obtained from the work by van Gemert *et al.* [145].

In the H-K model, a ray enters the material and it is repeatedly propagated from one scattering event to the next. Each scattering event attenuates the weight associated with the ray by a fixed factor which corresponds to the albedo. If the ray is not absorbed, it will eventually be scattered out of the material. In this last scattering event, the ray may leave the layer. In this case, according to Hanrahan and Krueger [54], the weight should be adjusted using the distance to the boundary. Hanrahan and Krueger did not explain how this adjustment should be performed, however. We remark, however, that final result is probably not going to be significantly affected by the weight adjustment with respect to the last interaction.

The procedure to be adopted when $sin\phi = 0$ was also left to the reader's interpretation perhaps for similar reasons. In this case one could simply discard the

current $\vec{s}$ for which $sin\phi = 0$, and compute another one. Since this situation is not likely to occur often, the possible implications in the final result would probably be negligible as well.

In the original paper [54] the warping function used to compute the cosine of the scattering angle has the term $|2g|$ in the denominator instead of $2g$, which effectively takes away the possibility of backscattering. This is quite acceptable for organic materials, which are characterized by forward scattering. If the parameter g is set to zero, the warping function reduces to $2\xi - 1$ where ξ corresponds to an uniformly distributed random number $\in [0, 1]$.

Hanrahan and Krueger did not provide details in their paper on how the Torrance-Sparrow model [134] was used to account for surface reflection on the outermost layers. However, since their framework is based on a stochastic ray tracing approach, one may consider that the Gaussian distribution of microfacets adopted in the Torrance-Sparrow model was used to obtain a warping function to perturb the reflected rays.

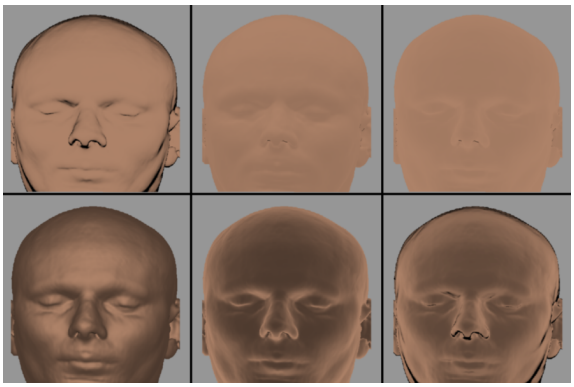

Figure 21: *Images illustrating the different parameters and approximations used in H-K model. Top column, from left to right: Fresnel effects, Seeliger's approximation, finite optical depth. Bottom column, from left to right: HGPF with* $g = -0.25$*, HGPF with* $g = 0.75$ *and a superposition of the Fresnel effects, finite optical depth and HGPF with* $g = 0.75$*. (Courtesy of Pat Hanrahan.)*

5.4. Strengths and Limitations

The H-K model has the merit of being one of the first computer graphics models to address important issues related to the simulation of light interaction with biological materials. However, because of its generality, it tends to overlook important specific characteristics and properties of organic materials, such as the mechanisms of absorption of light by natural pigments and their specific absorption coefficients. In the H-K model, these aspects are considered only implicitly through the use of coefficients available in the biomedical literature, which, in turn, were obtained using inversion procedures (Section 4.1). Hence, the reflectance and transmittance of skin specimens are not computed directly, but implicitly introduced into the model as the albedo. In other words, the H-K multiple-layer model has to be considered as a scattering model, instead of a reflectance model, since reflectance and transmittance values are not provided by the model.

The H-K model is isotropic, *i.e.*, it only considers the polar angle of the light incident on the material's surface. As described earlier, Hanrahan and Krueger indicated that their model can be combined with the Torrance-Sparrow model [134] in order to take into account the surface reflection on the outermost layers. The latter was, however, designed based on experimental data for inorganic materials, and its parameters are not biologically meaningful. Thus, it is not clear what criteria should be used in the selection of its parameters in order to model light interaction with organic materials.

The use of the HGPF in the subsurface scattering simulation of skin tissues raises some issues as well. First, its main parameter, the asymmetry factor, has no direct connection with the underlying biophysical phenomena. Second, the HGPF was initially meant to be used in tissue optics just as a function to fit multiple scattering data of skin measured at specific wavelengths by Bruls and van der Leun [19] (Section 2.2.2). Recently, Baranoski *et al.* [8] demonstrated that the HGPF approximations deviate from the measured data, and its generalized application to any organic tissue at any wavelength may lead to incorrect results, specially using asymmetry factors determined by fitting the HGPF to specific data sets that may have no relationship with the material at hand.

The evaluation of the H-K model did not include comparisons of model predictions with actual measured data, and it was based only in the visual inspection of computer generated images. More specifically, Hanrahan and Krueger provided images illustrating the application of different modeling features (Figure 21), and compared images rendered using the H-K model with images rendered using a Lambertian model (Figure 22). They also generated images of a human face whose different colors were rendered using texture maps to arbitrarily control pigment coefficients (Figure 23). We remark, however, that actual specific absorption spectra of different skin pigments were not used in the simulations.

In 2001, Ng and Li [93] proposed an extension to the H-K model which consists in adding a sebum layer on

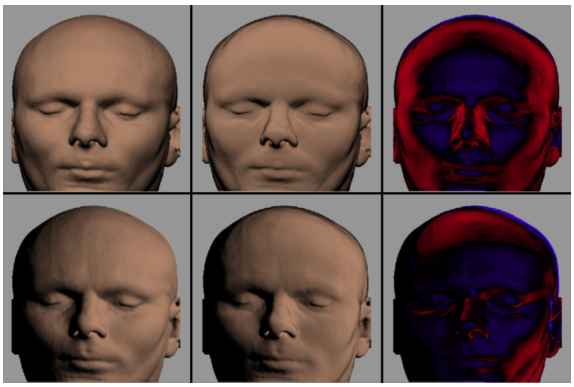

Figure 22: *Comparisons of images generated using a Lambertian model with images generated using the H-K model, and considering two angles of incidence, namely* 0° *(top row) and* 45° *(bottom row). Left column: Lambertian model. Middle column: H-K model. Right column: relative difference of both models, with the red color indicating more reflection from the new model, and the blue color indicating the opposite. (Courtesy of Pat Hanrahan.)*

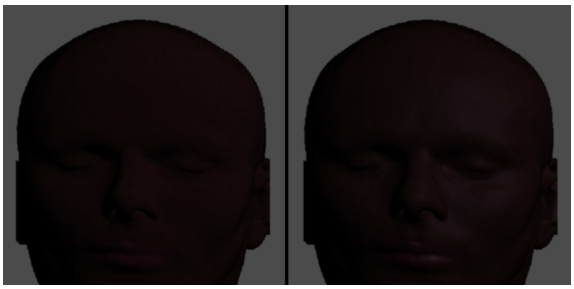

Figure 23: *Images illustrating the simulation of dark complexion by setting the Epidermis absorption coefficient to 0.6, and using the HGPF with* $g = 0.65$*. Left: considering only subsurface scattering. Right: adding a specular term to simulate an oil coat. (Courtesy of Pat Hanrahan.)*

the top of the epidermis layer. The work of Ng and Li has the merit of providing comparisons with actual measured data. Although the H-K model cannot be considered a predictable model, it can be used to render believable images of human skin (Figure 24), and it has raised the bar for computer graphics research involving organic materials.

6. The Discrete-Ordinate Model

The discrete-ordinate model proposed by Stam [124], henceforth referred to as D-O model, was developed to simulate the scattering behavior of skin. Spectral

Figure 24: *Image of an human face generated using the H-K model considering an oily outer layer and performing a Gaussian variation of parameters to create "freckles". (Courtesy of Pat Hanrahan.)*

quantities related to skin reflectance and transmittance are introduced into the model as input parameters, *i.e.*, mechanisms of light absorption by natural pigments were only implicitly considered. Although this biologically motivated model adopts a simplified representation for skin structure and optical properties, its deterministic algorithms for the simulation of light transport can represent a viable alternative for rendering applications that demand high interactive rates. Furthermore, the D-O model can be used to simulate light interactions with other materials. It is, however, examined in this tutorial in the context of skin rendering.

6.1. Overview

In the D-O model formulation, skin is represented by a single layer with constant optical properties and an uniform index of refraction. In addition, this layer is bounded by media having uniform indices of refraction as well (Figure 25). Following Hanrahan and Krueger [54], the D-O model considers that the skin depth is along the z-direction, and the skin properties are uniform in each xy-plane, *i.e.*, the skin is horizontally uniform. The parameters used to model the skin layer are the optical depth, the albedo and the asymmetry factor of the phase function (HGPF). Each parameter used in the D-O model is dimensionless, and varies from zero to one.

The D-O model also uses a parameter to account

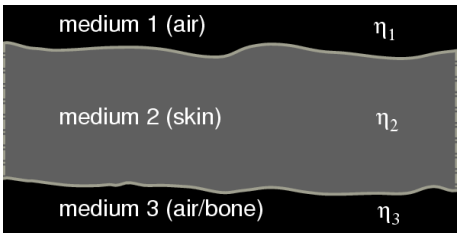

Figure 25: *Sketch describing the skin representation used by the D-O model, where the skin is represented by layer with an uniform index of refraction (η_2) bounded by two media with uniform refractive indices (η_1 and η_3) as well.*

for the roughness of the surfaces bounding the skin layer. This parameter controls the spatial distribution of light propagated at these interfaces. Incidentally, the surface roughness is assumed to be isotropic, *i.e.*, only the polar (elevation) angle of the light incident on the rough surfaces matters. Hence, we can classify the D-O model as isotropic as well.

6.2. Scattering Simulation

In order to model a skin layer bounded by rough surfaces, Stam extended the work by Stamnes and Conklin [125] for a skin layer bounded by a smooth surface, which is based on the discrete-ordinate approximation of radiative transfer equation [22]. The method of discrete-ordinates divides the radiative transport equation into n discrete fluxes to obtain n equations with n unknowns [103]. These equations are solved numerically by Stam [124] using Fourier transforms and eigenanalysis [49]. His approach was inspired by the work of Jin and Stammes [68].

6.2.1. Surface Reflection

The D-O model takes into account the reflection and refraction from the rough surfaces by extending the BRDF model proposed by Cook and Torrance [27], and following the work of van Ginneken *et al.* [148] in which the surfaces are assumed to have a normal distribution of heights. The reflection due to an ambient light source is modeled by integrating, over all incident directions, the BRDF due to scattering in the skin's layer whose computation is described in the next section.

6.2.2. Subsurface Reflection and Transmission

In the formulation used in D-O model, the radiance within the skin is obtained by considering its variation in an infinitesimal cylinder according to the following equaton:

$$-\zeta\frac{dL}{d\varrho} = -L + \frac{\gamma}{4\pi}\int_{4\pi}\Gamma(\vec{v}_s,\vec{v})L(\varrho,\vec{v}_s)d\vec{v}_s \qquad (22)$$

where:

L	=	radiance,
γ	=	albedo,
ζ	=	cosine of the polar scattering angle,
ϱ	=	optical depth,
$\vec{v}$	=	incident direction,
$\vec{v}_s$	=	scattering direction,
$\Gamma(\vec{v}_s,\vec{v})$	=	phase function.

Equation 22 is solved taking into account boundary conditions that related the BRDF and BTDF values, represented by r_{ij} and t_{ij} respectively (Figure 26), with radiance values at the air$\Longleftrightarrow$skin interfaces. Initially, the reflection and transmission operators, represented by R_{ij} and T_{ij} respectively, are defined as:

$$R_{ij}\{L\}(\varrho,\pm\vec{v}) = \int_{2\pi} r_{ij}(\mp\vec{v}_s,\pm\vec{v})L(\varrho,\mp\vec{v}_s)\zeta' d\vec{v}_s \qquad (23)$$

and

$$T_{ij}\{L\}(\varrho,\pm\vec{v}) = \int_{2\pi} t_{ij}(\mp\vec{v}_s,\pm\vec{v})L(\varrho,\mp\vec{v}_s)\zeta' d\vec{v}_s \qquad (24)$$

Then, the boundary condition at the skin surface ($\varrho = 0$) is given by:

$$L(0,-\vec{v}) = t_{12}(-\vec{v}_0,-\vec{v}) + R_{21}L(0,-\vec{v}) \qquad (25)$$

where:

$-\vec{v}_0$	=	direction of light incident on the air$\Longleftrightarrow$skin interface.

The boundary condition at the bottom ($\varrho_b = 0$), assuming that there are no sources below the skin, is given by:

$$L(\varrho_b,\vec{v}) = R_{23}\{L\}(\varrho_b,\vec{v}) \qquad (26)$$

Finally, the BRDF due to subsurface scattering is given by:

$$r_s(-\vec{v}_0,\vec{v}) = T_{21}\{L\}(0,\vec{v})/\zeta_0 \qquad (27)$$

where:

ζ_o	=	cosine of the polar scattering angle with respect to $-\vec{v}_0$.

Similarly, the BTDF due to subsurface scattering is given by:

$$t_s(-\vec{v}_0,-\vec{v}) = T_{23}\{L\}(\varrho_b,-\vec{v})/\zeta_0 \qquad (28)$$

The skin's BRDF and BTDF represented by Equations 27 and 28 are discretized with respect to a number of sample directions. This discretization process

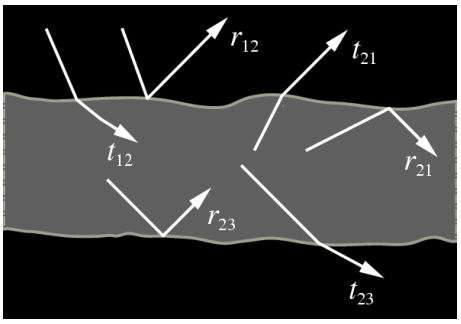

Figure 26: *Sketch describing the BRDF and BTDF interactions, represented by r_{ij} and t_{ij} respectively, taken into account into the D-O model.*

results in a collection of matrices that are precomputed for different values of the parameters used in the D-O model. During this process the phase functions, the HGPF, is expanded into a cosine series whose coefficients are expressed in terms of Legendre functions [22, 141, 142]. The corresponding system of equations representing n discrete fluxes described by n equations with n unknowns is solved numerically using Fourier transforms and eigenanalysis [49].

6.3. Implementation Issues

The precomputation of the matrices generates a large data set. In order to allow a practical use of this data in rendering frameworks, Stam [124] compressed it using an approximation based on cosine lobes. The cosine terms were chosen by visually comparing the data to the approximation. The data set was then further compressed by fitting a cubic Bèzier surface to the data stored in the reflection and transmission matrices. The control vertices of the Bèzier surfaces were constrained to respect their symmetry, *i.e.*, to obey the Helmholtz reciprocity rule[‖‖].

Stam [124] used the EISPACK [26] and LINPACK [33] numerical linear algebra packages to solve the system of equations. Alternatively, one could use their successor LAPACK [37]. Also, Stam made the D-O model implementation available as a shader plugin for the rendering software package Maya [102].

6.4. Strengths and Limitations

The D-O model is only a scattering model since reflectance and transmittance quantities are not computed. Although it is biologically-motivated, it does not take into account the structural characteristics of skin tissues and the biological processes that affect propagation and absorption of light in these tissues. The oversimplification of these biological processes, however, is not accompanied by the mathematical complexity of the algorithms used in the D-O model. Although these are not as complex as the rare analytical solutions for radiative transfer problems found in the literature, they are certainly less straightforward than the algorithms used in Monte Carlo based models. The main advantage of the D-O model over stochastic approaches using Monte Carlo methods is speed, which is sustained using precomputation and compressing schemes. We remark that the outputs of Monte Carlo based models can also be precomputed and compressed off-line, and reconstructed during rendering, reducing their operational costs.

On a rough surface it is possible that some points will not receive light, a phenomenon known as the shadowing effect. The D-O model takes into account this phenomenon, which is rarely incorporated in computer graphics models of light interaction with organic materials. As mentioned above, in order to accomplish that, Stam extended the Cook and Torrance model [27] using a shadowing function proposed by van Ginneken *et al.* [148]. It is worth noting that both models were mainly aimed at inorganic or man made materials, and their applicability to biological materials has not been verified.

The discrete-ordinates approach to solve radiative transfer problems is suitable when the material phase function can be expressed as a sum of a few terms [103]. The HGPF used in the D-O model can be expanded in a cosine series, whose coefficients are expressed in terms of Legendre functions [22]. This allows a relatively quick solutions for the radiative transfer equations. However, as pointed out before (Sections 4.5 and 5.4), the use of the HGPF in tissue optics is questionable in terms of its effects on the accuracy and predictability of the simulations.

The original description of the D-O model [124] does not include any comparison with measured data, only qualitative comparisons. For example, an image generated using the D-O model was compared to images generated using a Lambertian model and the H-K model (Figure 27) to illustrate the model's suitability for rendering applications. The differences were noticeable, but they were not as dramatic as one might expect from comparing images rendered using models with such different levels of complexity. Despite these aspects, the D-O model can be used to render believable images of humans (Figure 28).

[‖‖] This condition states that the BRDF for a particular point and incoming and outgoing directions remains the same if these directions are exchanged [94].

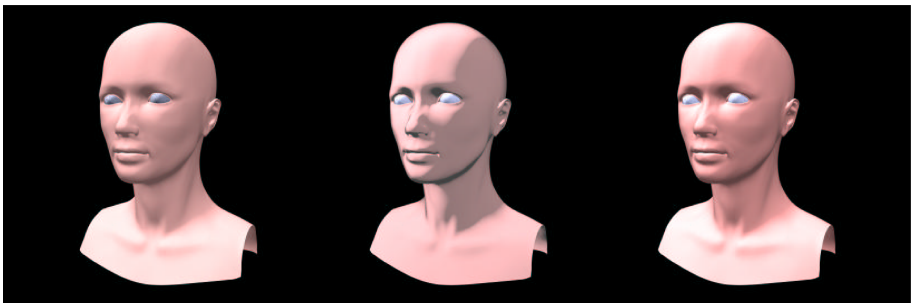

Figure 27: *Images generated using the D-O model (left), a Lambertian Model (middle) and the H-K model (right). (Courtesy of Jos Stam).*

Figure 28: *Image of a human head generated using the D-O model and applying texture maps to simulate lips and freckles. (Courtesy of Jos Stam).*

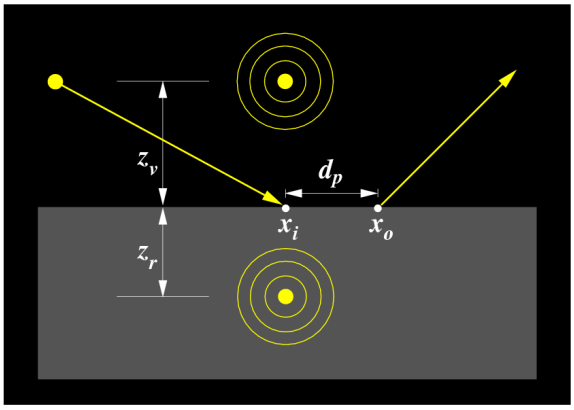

Figure 29: *Sketch describing the geometry used in the transformation of an incoming ray into a dipole source according to the diffusing theory approximation. The distances from the real and virtual dipole sources to the air⇔material interface are giving by z_r and z_v respectively, and the distance from the incidence point x_i to the propagation point x_o is giving by d_p.*

7. The Diffusion Theory Based Model

Jensen *et al.* [67] proposed a model for simulating the appearance of diffusive materials which applies the diffusion theory (Section 4.3) to account for subsurface light transport. In their model, henceforth referred to as D-T model, the general concept of the BSSRDF (Section 2.6) is used to describe the transport of light from one point on a surface to another. The performance of the D-T model was later improved by Jensen *et al.* through the incorporation of a two-pass hierarchical algorithm [65]. Although the D-T model was applied to the rendering of a variety of materials, from marble to milk, the following discussion focuses on applications involving human skin.

7.1. Overview

Jensen *et al.* [67] observed that, due to the effects of repeated multiple scattering, the light distribution tends to become symmetric (equal in all directions) and blurred in highly scattering media. Since the diffusion theory does not have a general analytical solution for finite media, they modeled subsurface reflection as a semi-infinite medium. They used the diffusion approximation for isotropic media known as the dipole method (Section 4.3) in which two point sources are placed relative to the surface, one representing the positive real light located below the surface, and the other representing a negative virtual light positioned above the surface. Using this approximation, they compute the radiant exitance at some propagation point separated by a certain distance from the incidence point (Figure 29).

The D-T model has four input parameters: the absorption coefficient, the reduced scattering coefficient, the diffuse reflectance and the index of refraction. In

order to determine the values of these parameters for various materials, they used a 3-CCD video camera to observe the radiant exitance across the surface of the material. They then used diffusion theory to compute the absorption coefficient and reduced scattering coefficient. In their follow-up work, Jensen and Buhler [65] reduced the space of parameters of the D-T model to the diffuse reflectance and an average scattering distance. It is also important to note that the follow-up work presents a more efficient scheme for sampling the incident flux due to subsurface scattering and does not alter the fundamentals or equations of the original work.

7.2. Surface Reflection

The D-T model is primarily a subsurface scattering model, and surface reflection is not directly addressed in its formulation. However, it can be combined with other models in order to handle surface reflection. For example, Jensen [66] mentioned the use of a Lambertian model in conjunction with the model proposed by Torrance and Sparrow model [134] in order to improve the realistic appearance of a human face rendered using the D-T model (Figure 41).

7.3. Subsurface Reflection

The D-T model is formally defined by Jensen *et al.* [67] as a sum of a single scattering term and the diffusion approximation. Jensen *et al.* proposed the use of an analytical approximation to account for single scattering events which may occur when a refracted incoming ray and an outgoing ray intersect. It consists in computing, using a formulation based on the analytical solution for first-order scattering proposed by Hanrahan and Krueger (Section 5.2.2), the light transport integral over a selected portion of path length along the direction of refraction (Figure 30).

For the diffusion approximation, Jensen *et al.* [67] proposed an algorithmic approach which can be summarized as follows:

1. generate a set of sampling points on the surface of the model,
2. for each sampling point compute the incident irradiance using any lighting algorithm, and
3. for each sample point compute the radiant exitance using the following equation which takes into account the geometry presented in Figure 29:

$$dM_o(x_o) = d\Phi_i(x_i)\frac{\gamma'}{4\pi}\left(C_1\frac{e^{-\mu_{tr}d_r}}{d_r^3} + C_2\frac{e^{-\mu_{tr}d_v}}{d_v^3}\right) \tag{29}$$

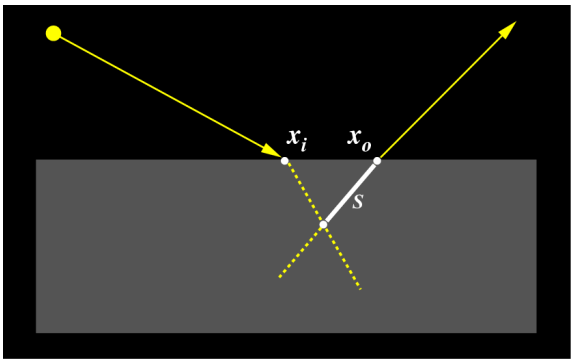

Figure 30: *Sketch describing the geometry used to account for single scattering which is computed as an integral over the path length S along the direction of refraction.*

with C_1 given by:

$$C_1 = z_r\left(\mu_{tr} + \frac{1}{d_r}\right)$$

and C_2 given by:

$$C_2 = z_v\left(\mu_{tr} + \frac{1}{d_v}\right)$$

where:

$d\Phi_i(x_i)$	=	incident flux at sampling point,
γ'	=	reduced albedo,
μ_{tr}	=	effective transport extinction coefficient,
d_r	=	distance from the propagation point x_o to the real dipole light source,
d_v	=	distance from the propagation point x_o to the virtual dipole light source,
z_r	=	distance from the incidence point x_i to the real dipole light source,
z_v	=	distance from the incidence point x_i to the real dipole light source.

The reduced albedo, γ', is given by:

$$\gamma' = \frac{\mu_s'}{\mu_t'} \tag{30}$$

where μ_s' corresponds to the reduced scattering coefficient (Section 2.3), and the reduced extinction coefficient, μ_t', is given by:

$$\mu_t' = \mu_s' + \mu_a \tag{31}$$

where:

μ_a	=	absorption coefficient.

The effective transport extinction coefficient, μ_{tr}, is given by:

$$\mu_{tr} = \sqrt{3\mu_a\mu_t'} \tag{32}$$

The distance to the real light source, d_r, is given by:

$$d_r = \sqrt{{d_p}^2 + z_r^2} \tag{33}$$

where:

d_p = distance from the propagation point x_o to the the incidence point x_i.

and the distance to the virtual light source, d_v, is given by:

$$d_v = \sqrt{{d_p}^2 + z_v^2} \tag{34}$$

The distance from the virual dipole light to the surface, z_v, is given by:

$$z_r = \frac{1}{\gamma'} \tag{35}$$

and the distance from the real dipole light to the surface, z_r, is given by:

$$z_v = z_r + 4\frac{1 + F_{dr}}{1 - F_{dr}}\frac{1}{3\varrho'_t} \tag{36}$$

where the Fresnel term F_{dr} corresponds to the average diffuse Fresnel reflectance. Jensen *et al.* [67] compute this term using an approximation for the internal diffuse reflectance proposed by Egan and Hilgeman [38] which is given by:

$$F_{dr} = -\frac{0.5601}{\eta_r^2} + \frac{0.710}{\eta_r} + 0.668 + 0.0636\eta_r \tag{37}$$

where

η_r = refractive index of the medium.

The expression for F_{dr} given in Equation 37 corresponds to a curve fit to tabular data provided by Orchard [97].

7.4. Implementation Issues

Our impression is that the description of the D-T model provided in the original paper by Jensen *et al.* [67] is a bit more complex than than the model itself. The formulation is cumbersome to follow at some points, and some details are left to the reader's interpretation. For example, although in the paper by Jensen *et al.* [67] the term η_r is defined as "the relative index of refraction of the medium with the reflected ray to the other medium", it is simply defined as "the index of the refraction of the medium" in the works by Groenhuis *et al.* [53] and by Egan and Hilgeman [38] cited by Jensen *et al.* [67]. Another example refers to Equation 29. In the original paper the exponent of the terms d_r and d_v is 3, while in the second paper by Jensen and Buhler [65] it is 2. Although this small discrepancy may be due to a simple typographical error, the derivation of this exponent is not clearly stated in the text.

We found the algorithmic description provided in the second paper by Jensen and Buhler [65] clearer and easier to follow. According to their description, the three main tasks involved in the implementation of the D-T model are:

1. the implementation of the diffusion approximation equations described above,
2. the computation of the sample points, and
3. the optimization of the algorithm through the use of an hierarchical technique.

The optimization proposed by Jensen and Buhler [65] consists in using an hierarchical data structure so that sample points can be selected by their relevance, and points that are distant can be grouped together. More specifically, Jensen and Buhler suggested the use of an octree for the implementation of this hierarchical acceleration mechanism. Alternatively, other data structures, such as a BSP-tree [45] or a kd-tree [14], could be used***

The approximation for F_{dr} proposed by Egan and Hilgeman [38], which appears in both papers [67, 65], has also been applied in the work by Groenhuis *et al.* [53] in the investigation of scattering and absorption in turbid materials. It is important to note that in both cases, *i.e.*, the papers describing the D-T model and the work by Groenhuis *et al.* cited in these papers, the formula for this approximation presents an error. More specifically, it has the constant -1.44 multiplying the ${\eta_r}^{-2}$ term instead of the constant -0.56 that appears in Equation 37. Incidentally, the formula given in Equation 37 was obtained directly from the expression provided by Egan and Hilgeman [38].

All aspects considered, we found the implementation of the tasks mentioned above to be relatively simple. This aspect makes the incorporation of the D-T model into rendering frameworks straightforward. Incidentally, Jensen *et al.* [67] have incorporated the D-T model in a Monte Carlo ray tracer.

7.5. Strengths and Limitations

The usual assumption made in tissue optics that light entering a material leaves the material at the same position is relaxed in the D-T model. From a theoretical point of view, this is a valid contribution since such an assumption fails to represent the real behavior of diffusive or translucent materials. In practice,

*** In our implementation of the D-T model, we performed experiments using the three data structures indicated in the text. Although our results may be biased by implementation issues, they suggest that octrees can perform better in this type of simulation.

however, the effects of this assumption on the appearance of the materials may not be as significant as the effects resulting from other assumptions such as the homogeneity of the materials. Furthermore, the errors introduced in a scattering simulation by the the elimination of the positional argument of the BSSRDF may be diluted or compensated when one applies stochastic simulation approaches. Even though the inclusion of such positional argument may contribute to the accuracy of the scattering simulations, such gain may be mitigated by the use of other approximations, such as the diffusion approximation itself, and other simplifying techniques such as the application of a curve fit formula to computed the Fresnel terms.

The D-T model is relatively simple to implement, general (can be used for different diffusive materials), and it is not as computationally expensive as Monte Carlo based models. In addition, it can be used to render visually pleasing images. These reasons may have motivated its incorporation (or some variant) in several commercial rendering packages. However, similarly to the H-K model, it presents some limitations associated to its generality. It does not take into account properties specific to organic materials. Also, like the H-K model, the input parameters come either from inversion procedures or can be arbitrarily set by the user (in the case of the simplified set of parameters [65]). Due to the fact that spectral properties such as the diffuse reflectance are actually input parameters to the model (obtained using an inversion procedure based on the use of video camera and diffusion theory), the D-T model shall be classified only as a scattering model.

The diffusion approximation used in the D-T model requires the computation of the reduced scattering coefficient (Section 2.3), which in turn uses as a parameter the asymmetry factor, g, of the phase function. Jensen *et al.* [67] apply the HGPF, and used $g = 0.85$ for the whole skin. We infer that this value comes from a paper that followed the work by Bruls and van der Leun [19] since no direct reference was provided by Jensen *et al.* [67]. In the second paper, Jensen and Buhler [65] used the HGPF with the asymmetry values provided by van Gemert *et al.* [145]. Besides the direct effect on the predictability and accuracy of the scattering simulations (Section 4.5, the use of the HGPF and the selection of asymmetry factors may have further theoretical implications. As claimed by Jensen *et al.* [67], according to Furutso [48], the diffusion approximation may be accurately applied when $\frac{\varrho_a}{\varrho_a+\varrho_s} << 1 - g^2$. Clearly, in order to apply this relationship, one needs to know the values of its terms, which in turn come from measured data. As discussed earlier (Section 2.3), the values of g available in the tissues optics literature, including the values mentioned above, usually come from fitting approaches, *i.e.*, they are already approximations. Furthermore, the data used as reference in these fitting approaches may refer to materials whose optical properties differ from the material at hand, which may even further decrease the accuracy of such approximations.

The D-T model considers the entire skin structure as one medium. As described in Section 3, skin is heterogeneous and layered, with each of the layers having different biological and optical properties (particularly the epidermis and dermis). It is reasonable to assume that diffusion approximation can be applied to simulating subsurface reflection in the dermis [147], however, there are some issues regarding its use for other skin layers. First, the diffusion approximation is not suitable when the scattering is mostly in the forward direction [44, 48, 159]. As mentioned in Section 3, the measurements performed by Bruls and van der Leun [19] demonstrate that both the stratum corneum and the epidermis tissues are highly forward scattering media. Second, as mentioned in Section 4.3 and quantitatively stated by Furutso [48], the diffusion theory is not applicable when the absorption coefficient is not significantly smaller than the scattering coefficient for turbid media. Recall that human skin is characterized by the presence of pigments, such as melanin particles, which have a significant absorption cross section [23]. This issue is particularly relevant for heavily pigmented specimens.

The evaluation of the D-T model and its variant is also based solely on visual inspection. Since comparisons to actual BRDF and BTDF data of any organic (or inorganic) material were not provided, neither the accuracy nor the predictability of the D-T model can be verified. Jensen *et al.* [67] compared an image generated using a BRDF model with an image generated using the D-T model (Figure 31). Although it is not clearly indicated in the original paper, it is suggested that a model similar to the H-K model (Section 5) was used as the BRDF model. The image generated using the D-T model presents noticeable blurring effects. However, since quantitative data is not provided, it is not clear whether or not similar effects could be obtained by simply perturbing the incident light rays. Despite these issues, the D-T model has been successfully used in the generation of believable images of human beings used in entertainment applications (Figure 32) and virtual face cloning (Figure 41). Moreover, the development of the D-T model has addressed the positional assumption made by the other models, and it has raised important theoretical issues concerning subsurface scattering simulations. Incidentally, the D-T model limitations mentioned above and in previous works by Baranoski and Krishnaswamy [8] and Baranoski *et al.* [6] have been acknowledged by Donner

Figure 31: *Images generated using a BRDF approximation (top) and the BSSRDF approximation provided by the D-T model (bottom). (Courtesy of Henrik Wann Jensen.)*

Figure 32: *Images of a textured face before (top) and after (bottom) the addition of the subsurface scattering simulation provided by the D-T model. (Courtesy of Henrik Wann Jensen.)*

and Jensen [34] in a recent paper describing a hybrid method for simulating the scattering profile of translucent materials using multiple dipoles and a variation of the K-M theory.

8. The Biophysically-Based Spectral Model

Many models used in computer graphics rely on spectral parameters, such as reflectance and transmittance, whose values are either arbitrarily set by the user or obtained from direct measurements or inversion procedures. There are measured reflectance curves for human skin available in the biomedical literature, but they are limited to a very specific set of skin types and restricted to a narrow range of illuminating and viewing angles. Furthermore, measured transmittance curves for the skin organ as a whole are scarce. These aspects highlight the need to develop models of light interaction with human skin which can compute not only its scattering properties (given in terms of BRDF and BTDF), but also its spectral properties (given in terms of reflectance and transmittance). The biophysically-based spectral model, henceforth referred to as BioSpec, was proposed by Krishnaswamy and Baranoski [75] to address this need. Since the BioSpec model takes into account biophysical processes affecting both the spectral and spatial distributions of light interacting with human skin, it is examined in this tutorial in some detail.

8.1. Overview

The BioSpec model uses ray optics and Monte Carlo techniques to simulate the processes of light propagation (surface reflection, subsurface reflection and transmission) and absorption in the skin tissues. It considers the stratification of skin into four semi-infinite main layers: stratum corneum, epidermis, papillary dermis, and reticular dermis. The model parameter space includes: the refractive index and thickness of each layer, the refractive index and the diameter of collagen fibrils, the extinction coefficient (Figure 9), concentration, and volume fraction of the main chromophores present in the skin tissues (eumelanin, phaeomelanin, oxyhemoglobin, deoxyhemoglobin, β-carotene and bilirubin) and the aspect ratio of the stratum corneum folds.

The propagation of light in the skin tissues is simulated as a random walk process [50], whose states are associated with the following interfaces:

1. air $\Leftrightarrow$ stratum corneum;
2. stratum corneum $\Leftrightarrow$ epidermis;
3. epidermis $\Leftrightarrow$ papillary dermis;
4. papillary dermis $\Leftrightarrow$ reticular dermis;
5. reticular dermis $\Leftrightarrow$ hypodermis.

Once a ray hits the skin specimen at interface 1, it can be reflected back or refracted into the stratum

corneum. From there, the ray can be reflected and refracted multiple times within the skin layers before it is either absorbed or propagated back to the environment thru interface 1. Recall that the hypodermis is a highly reflective medium (Section 3.2). For this reason, for body areas characterized by the presence of this tissue, the BioSpec algorithmic formulation assumes total reflection at interface 5.

In the random walk implemented by the BioSpec model, the transition probabilities are associated with the Fresnel coefficients [9] computed at each interface (assuming that the cells are locally flat, *i.e.*, they are large with respect to the wavelength of the incoming light), and the termination probabilities are associated with the free path length (p) computed when a ray travels in the skin layers.

8.2. Scattering Simulation

The BioSpec model takes into account the three components of a skin specimen's BDF: surface reflectance, subsurface reflectance and transmittance. These components are affected by the refractive indices differences at the interfaces, tissue scattering and absorption of light by skin pigments. In the next sections we describe how each of these components is simulated. Due to the stochastic nature of the simulations, several random numbers uniformly distributed in the interval $[0, 1]$ and represented by ξ_i (for $i = 1..14$) are employed in the BioSpec formulation.

After computing the Fresnel coefficient (F) at an interface, a random number ξ_1 is obtained. If $\xi_1 \leq F$, then a reflected ray is generated, otherwise a refracted ray is generated. The reflected ray is computed applying the law of reflection, and the refracted ray is computed applying Snell's law [56].

8.2.1. Surface Scattering

A portion of the light that interacts with the stratum corneum cells is reflected back to the environment following the computation of the Fresnel coefficients described above. The spatial distribution of the reflected light varies according to the aspect ratio of the stratum corneum folds (Section 3.3). In the BioSpec model, these mesostructures are represented as ellipsoids whose aspect ratio ($\sigma \in [0, 1]$) is defined as the quotient of the length of the vertical axis by the length of the horizontal axis, which are parallel and perpendicular to the specimen's normal respectively. As the folds become flatter (lower σ), the reflected light becomes less diffuse. In order to account for this effect, the reflected rays are perturbed using angular displacements obtained from the surface-structure function proposed by Trowbridge and Reitz [135], which represents rough air-material interfaces using microareas randomly curved. These displacements [75, 74] are given in terms of the polar perturbation angle:

$$\alpha_S = \arccos\left[\left(\left(\frac{\sigma^2}{\sqrt{\sigma^4 - \sigma^4\xi_2 + \xi_2}} - 1\right) b\right)^{\frac{1}{2}}\right] \quad (38)$$

where:
$b = \frac{1}{\sigma^2 - 1}$,

and the azimuthal perturbation angle:

$$\beta_S = 2\pi\xi_3 \quad (39)$$

8.2.2. Subsurface Scattering

Scattering in either the stratum corneum or epidermis involves the perturbation of the incoming ray in both the polar (α_f) and azimuthal (β_f) angles. The scattering with respect to the azimuthal angle β_f is expected to be symmetric (equal in all directions) [104], thus $\beta_f = 2\xi_4\pi$ is used. The scattering direction with respect to the polar angle α_f is computed using a randomized table look-up algorithm. The polar scattering angles measured at a given wavelength by Bruls and Leun [19] (Section 3.3) are stored in a table, whose access indices correspond to the measured fractions of scattered radiation. For each ray a random number ξ_5 is generated, which is multiplied by the table size. The integer part of the resulting value is used to access the corresponding polar scattering angle stored in the table.

Every ray entering one of the dermal layers is initially tested for Rayleigh scattering (Section 2.2.2). If the test fails or the ray has already been bounced off one of the dermal interfaces, then the ray is randomized around the normal direction using a warping function based on a cosine distribution [9], in which the polar perturbation angle, α_c, and the azimuthal perturbation angle, β_c are given by:

$$(\alpha_c, \beta_c) = (\arccos((1 - \xi_8)^{\frac{1}{2}}), 2\pi\xi_9) \quad (40)$$

In order to perform the Rayleigh test, the spectral Rayleigh scattering amount, $R_{sca}(\lambda)$, is computed (Equation 42). This spectral quantity is associated with the probability that the Rayleigh scattering can occur [85]. A random number ξ_{10} is then generated, and if $\xi_{10} < 1 - \exp^{-R_{sca}(\lambda)}$, the ray is scattered using polar (α_R) and azimuthal (β_R) perturbation angles. The perturbation angles are given by:

$$(\alpha_R, \beta_R) = (\psi, 2\pi\xi_{11}) \quad (41)$$

where the angle ψ is obtained using rejection sampling

in conjunction with the Rayleigh phase function [85]:

$$\begin{array}{ll} do & \\ & \psi = \pi\xi_{12} \\ & \chi = \frac{3}{2}\xi_{13} \\ while & (\chi > \frac{3}{4}(1+\cos^2\psi)) \end{array}$$

Note that ξ_{12} and ξ_{13} must be regenerated during each iteration of the loop described above.

According to Jacques [63], collagen fibers occupy 21% of the dermal volume, and the Rayleigh scattering in this tissue can be approximated using spheres mimicing the ultrastructure associated with the random arrays of collagen fibrils of radius r_f. This results in a fiber density $N = \frac{4}{3} * r_f^3 * 0.21$. This value is used in the BioSpec formulation to compute the spectral Rayleigh scattering amount [74, 85] through the following equation:

$$R_{sca}(\lambda) = \frac{8\pi^3 \left(\left(\frac{\eta_f}{\eta_m}\right)^2 - 1 \right)^2}{3N\lambda^4} \left(\frac{h}{\cos\theta} \right) \qquad (42)$$

where:

η_f	=	index of refraction of the fibers,
η_m	=	index of refraction of the dermal medium,
h	=	thickness of the medium,
θ	=	angle ($< 90°$) between the ray and the specimen's normal.

8.3. Absorption

When a ray travels in a given layer, it is first scattered as described in the previous section. The ray is then tested for absorption. If the ray is not absorbed, then it is propagated to the next layer. The absorption testing done by the BioSpec model is based on Beer's law (Section 2.5). It is performed probabilistically every time a ray starts a run in a given layer. It consists of estimating the ray free path length (p) through the following expression:

$$p(\lambda) = -\frac{1}{\zeta_{t_i}(\lambda)} \ln(\xi_{14}) \cos\theta \qquad (43)$$

where:

$\zeta_{t_i}(\lambda)$	=	total absorption coefficient of the pigments of given layer i,
θ	=	angle between the ray and the specimen's normal.

If $p(\lambda)$ is greater than the thickness of the pigmented medium, then the ray is propagated, otherwise it is absorbed.

The BioSpec model accounts for the presence of eumelanin, phaeomelanin, oxyhemoglobin, deoxyhemoglobin, bilirubin and β-carotene. The spectral extinction coefficients for these pigments, denoted $\epsilon_{eu}(\lambda)$, $\epsilon_{ph}(\lambda)$, $\epsilon_{ohb}(\lambda)$, $\epsilon_{dhb}(\lambda)$, $\epsilon_{bil}(\lambda)$ and $\epsilon_{car}(\lambda)$ respectively, are obtained from the curves shown in Figure 9. The total absorption coefficient for each layer is simply the sum of the specific absorption coefficients (s.a.c.) of each pigment present in the layer, which are obtained by multiplying the pigment's spectral extinction coefficient by its estimated concentration in the layer.

It is difficult to accurately determine the baseline absorption coefficient for pigmentless skin tissues. Furthermore, due to its low magnitude [111] compared to the absorption coefficients of the skin chromophores, skin optics researchers usually assume that its effects are negligible [3]. For the sake of completeness, however, the baseline skin absorption coefficient, $\zeta_{base}(\lambda)$, was included in the absorption equations used in the BioSpec model.

The stratum corneum total absorption coefficient is given by:

$$\zeta_1(\lambda) = \zeta_{base}(\lambda) + \zeta_{cs}(\lambda) \qquad (44)$$

where:

$\zeta_{cs}(\lambda)$	=	β-carotene s.a.c.

The β-carotene s.a.c. is given in Equation 1.

The epidermis total absorption coefficient is given by:

$$\begin{aligned} \zeta_2(\lambda) = & \left(\zeta_{eu}(\lambda) + \zeta_{ph}(\lambda)\right)\vartheta_m \\ & + (\zeta_{base}(\lambda) + \zeta_{ce}(\lambda))(1 - \vartheta_m) \end{aligned} \qquad (45)$$

where:

$\zeta_{eu}(\lambda)$	=	eumelanin s.a.c.,
$\zeta_{ph}(\lambda)$	=	phaeomelanin s.a.c.,
$\zeta_{ce}(\lambda)$	=	β-carotene s.a.c. in the epidermis,
ϑ_m	=	volume fraction (%) of the epidermis occupied by melanosomes $\div 100$.

The eumelanin s.a.c. is given by:

$$\zeta_{eu}(\lambda) = \epsilon_{eu}(\lambda) c_{eu} \qquad (46)$$

where:

c_{eu}	=	eumelanin concentration ($\frac{g}{L}$).

Similarly, the phaeomelanin s.a.c., $\zeta_{ph}(\lambda)$, is computed by multiplying its spectral extinction coefficient, $\epsilon_{ph}(\lambda)$, by its concentration, c_{ph}. Also, the absorption coefficient ζ_{ce} is obtained by replacing c_{cs} by the concentration of β-carotene, c_{ce}, in Equation 1.

The papillary dermis total absorption coefficient is given by:

$$\zeta_3 = (\zeta_{ohb}(\lambda) + \zeta_{dhb}(\lambda) + \zeta_{cd}(\lambda) + \zeta_{bil}(\lambda))\,\vartheta_p + \zeta_{base}(\lambda)(1-\vartheta_p) \quad (47)$$

where:

$\zeta_{ohb}(\lambda)$	=	oxyhemoglobin s.a.c.,
$\zeta_{dhb}(\lambda)$	=	deoxyhemoglobin s.a.c.,
$\zeta_{cd}(\lambda)$	=	β-carotene s.a.c. in the dermal layers,
$\zeta_{bil}(\lambda)$	=	bilirubin s.a.c.,
ϑ_p	=	volume fraction (%) of the papillary dermis occupied by whole blood $\div 100$.

The β-carotene s.a.c., ζ_{cd}, in the dermal layers is obtained by replacing c_{cs} by the concentration of β-carotene in the dermal layers (c_{cd}) in Equation 1. Also, recall that the volume fractions of blood vary within the dermis tissue (Section 3.2). Hence, to compute the reticular dermis total absorption coefficient, ζ_4, the volume fraction ϑ_p is replaced by ϑ_r (volume fraction (%) of the reticular dermis occupied by whole blood $\div 100$) in Equation 47.

The oxyhemoglobin s.a.c. is given by:

$$\zeta_{ohb}(\lambda) = \frac{\epsilon_{ohb}(\lambda)}{66500} c_{hb} * \varphi \quad (48)$$

where:

66500	=	molecular weight of hemoglobin $(g/mole)$,
c_{hb}	=	concentration of hemoglobin in the blood $(\frac{g}{L})$,
φ	=	ratio of oxyhemoglobin to the total hemoglobin concentration.

Similarly, the deoxyhemoglobin s.a.c., $\zeta_{dhb}(\lambda)$, is computed using its spectral extinction coefficient, $\epsilon_{dhb}(\lambda)$, and replacing φ by $(1-\varphi)$ in Equation 48.

Finally, the bilirubin s.a.c. is given by:

$$\zeta_{bil}(\lambda) = \frac{\epsilon_{bil}(\lambda)}{585} c_{bil} \quad (49)$$

where:

585	=	molecular weight of bilirubin $(g/mole)$,
c_{bil}	=	bilirubin concentration $(\frac{g}{L})$.

8.4. Implementation Issues

Since the BioSpec model uses an algorithmic formulation based on standard Monte Carlo techniques, it can be seamlessly incorporated into rendering libraries such as the *ggLibrary* [120], a set of *C++* utilities designed to be used in computer graphics applications. In the *ggLibrary*, materials are classified as families such as metals and dielectrics, and grouped by parameters that affect their behavior, following the ray tracing framework for global illumination proposed by Shirley and Sung [121]. A set of routines specific for each family computes the BDF for that family. In the case of the BioSpec model, the new *ggLibrary* family corresponds to skin tissues, and each of the five states of the random walk process is implemented through a different routine. These routines are called recursively by a controlling routine until the ray is either absorbed or propagated to the environment.

One of the main challenges for users of comprehensive models such as the BioSpec model refers to data acquisition. In order to mitigate this problem, the data used in the BioSpec formulation was made available online[***].

As described earlier, to perturb the ray reflected on the skin surface, Krishnaswamy and Baranoski [75] used angular displacements obtained from the surface-structure proposed by Trowbridge and Reitz [135]. Alternatively a warping function based on an exponentiated cosine function [9] could be tested. Earlier experiments by Blinn [16] showed that curves resulting from the function proposed by Trowbridge and Reitz and curves resulting from exponentiated cosine functions have a similar shape. Incidentally, the formula for the polar perturbation angle, α_s, given in the original paper describing the BioSpec model [75] presents a typographical error, namely the position of the exponent $\frac{1}{2}$. This error was fixed in Equation 38 presented above.

The formula for the polar perturbation angle, α_s, represents only an approximation [74] since the integration of function proposed by Trowbridge and Reitz and its subsequent inversion to obtain α_s is not computationally practical. We remark, however, that it is possible to use a data driven mechanism (such as the table look-up used to simulate the subsurface scattering the stratum corneum and epidermis layers) to compute the perturbation angle. Such an approach would have the benefits of being more accurate since it would use values provided by the original function proposed by Trowbridge and Reitz, and being faster than applying Equation 38 on the fly.

8.5. Strengths and Limitations

BioSpec, to the best of our knowledge, is the first computer graphics model capable of computing both scattering and spectral quantities for skin specimens. Its implementation based on standard Monte Carlo methods enables its straightforward implementation. The algorithmic simulations performed by the model,

*** http://www.aravind.ca/downloads/BioSpecSkinData.h

however, are time consuming and may represent a bottleneck in an image synthesis pipeline. Alternatively, these simulations can be run off-line, and the quantities computed by the model stored and reconstructed during rendering.

On the scientific side, there is still room for improvement in the BioSpec formulation. For example, similarly to previous models [54, 93, 67], shadowing and masking effects are not taking into account by the BioSpec model. Also, although the simulation of surface reflection performed by the BioSpec model accounts for biological factors and employs a closer approximation to the skin mesostructures' aspect ratio than approaches based on the use of microfacets [54, 124], its generalization requires a more rigorous mathematical treatment [74]. Furthermore, in the BioSpec formulation, it is assumed that all rays are reflected at the dermis$\Longleftrightarrow$hypodermis interface. Such an assumption may need to be relaxed since it has not been fully verified through actual experiments. In fact, it is still an open question in tissue optics.

The BioSpec model was evaluated through comparisons with spectral and scattering measured data. Figure 33 presents comparisons of modeled reflectance curves provided by the BioSpec model with actual measured curves provided by Vrhel *et al.* [150] (available in the North Carolina State University (NCSU) spectra database) for lightly and moderately pigmented specimens. The measurements were performed considering $\theta_i = 45^\circ$ [150].

Figure 34 presents comparisons between modeled and actual measured transmittance curves for the stratum corneum and epidermis tissues of two specimens, a moderately and a heavily pigmented one. The measured transmittance data for human skin available in the scientific literature is usually limited to separated skin layers. Krishnaswamy and Baranoski [75] used measured curves (with a reported tolerance of $\approx \pm 5\%$) provided by Everett *et al.* [40], which were obtained at a normal angle of incidence ($\theta_i = 0^\circ$). Everett *et al.* [40] reported thickness values for the moderately pigmented ($t_s = 0.0017cm$ and $t_e = 0.0025cm$) and the heavily pigmented ($t_s = 0.0023cm$ and $t_e = 0.0021cm$) specimens. Based on their description of the specimens, Krishnaswamy and Baranoski [75] set $\vartheta_m = 9.5\%$ and $\vartheta_m = 38\%$ for the lightly and heavily specimens respectively.

The quantitative discrepancies between modeled and measured results may be due in part to the fact that the some parameters used in the simulations had to be estimated based on the overall description of the specimens and others correspond to average values found in the literature (*e.g.*, the refractive indices for the skin layers). Furthermore, the exact position of the absorption peaks of natural pigments depends on the solvents in which they are dissolved, and one can expect small shifts when comparing to *in vivo* values [62]. Clearly, such data limitations affect the accuracy of modeled curves. Nonetheless, even though the modeled spectral curves provided by the BioSpec model show good quantitative agreement with measured curves, more experiments with differents types of skin specimens and different measurement geometries are required to fully determine the robustness of the BioSpec algorithmic formulation.

Figure 35 shows a comparison between modeled and actual measured skin BRDFs provided by Marschner *et al.* [84]. Based on the lightly pigmented specimen's description provided by Marschner *et al.* [84], Krishnaswamy and Baranoski [75] set $\vartheta_m = 2.5\%$ in these experiments. As illustrated by the measurements provided by Marschner *et al.* [84] (Figure 35 (top)), the BRDF of skin specimens presents an angular dependence, and it becomes more diffuse for small angles. Figure 35 (bottom) shows that the BioSpec model can represent this angular dependency, and the modeled BRDF curves generally agree with the measured BRDF curves provided by Marschner *et al.* [84]. The most noticeable quantitative discrepancies are observed for the larger angle of incidence, namely $\theta_i = 60^\circ$. It is worth noting, however, that besides the previously mentioned factors that quantitatively affect the modeled curves, one should also consider the sources of noise in the measurements performed by Marschner *et al.* [84], which include deviations in the specimen's normal estimation and spatial variations in the measured BRDFs.

Since quantitative evaluations may be affected by inherent difficulties to characterize testing specimens, oftentimes qualitative evaluations may help to provide a better assessment of a model's predictive capabilities. Promising evidence of such capabilities was provided by the qualitative agreement between the modeled results provided by the BioSpec model and observed phenomena. For example, the overall reflectance of human skin presents interesting features. As expected, darker skin (characterized by higher volume fractions of epidermis occupied by melanosomes) reflects less light than lighter skin. However, lightly pigmented skin presents a characteristic "W" shape in the reflectance curves between $500nm$ and $600nm$ [3]. Oxygenated hemoglobin is responsible for this feature, which can be accentuated as the proportion of oxyhemoglobin with respect to total hemoglobin increases [161]. The graphs presented in Figure 36 indicates that the BioSpec model can capture these optical characteristics of human skin. Another example refers to skin BRDF. Skin specimens characterized by thin and numerous folds (*e.g.*, young and/or hydrated spec-

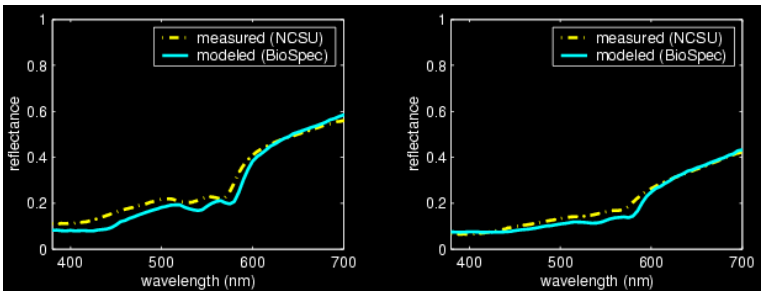

Figure 33: *Comparison of modeled reflectance curves provided by the BioSpec model with actual measured curves available in the NCSU spectra database by Vrhel [1994]. Left: lightly pigmented skin specimen (NCSU file 113). Right: moderately pigmented specimen (NCSU file 82).*

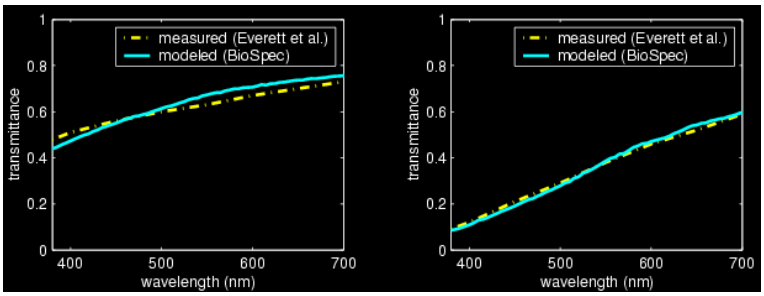

Figure 34: *Comparison of modeled transmittance curves (for the stratum corneum and epidermis tissues) provided by the BioSpec model with actual measured curves provided by Everett et al. [40]. Left: moderately pigmented specimen. Right: heavily pigmented specimen.*

imens) present a directional behavior stronger than specimens with wider but fewer folds (*e.g.*, old and/or dry specimens) [84, 130, 132]. The former case corresponds to folds with lower aspect ratio, while the later case corresponds to folds with a higher aspect ratio [130, 132]. Figure 37 presents modeled BRDF curves for two angles of incidence, namely $\theta_i = 15°$ and $\theta_i = 45°$, obtained by varying the parameter σ associated with the folds' aspect ratio. These curves show that the BioSpec model can qualitatively simulate the variation in the scattering behavior of skin specimens associated with changes in the aspect ratio of the stratum corneum folds.

Besides the experimental evaluation, Krishnaswamy and Baranoski [75] also rendered images to illustrate the applicability of the BioSpec model in the spectral simulation of medical conditions, *e.g.*, jaundice (Figure 38) and erythema (Figure 39), associated with changes in the biophysical parameters, and to highlight an aspect for which measured data is scarce, namely the translucency of skin tissues (Figure 40). The transmission of light through the whole skin can be observed (*in vivo*) in body parts with a thin or absent hypodermis, such as ears, eye lids and fingers.

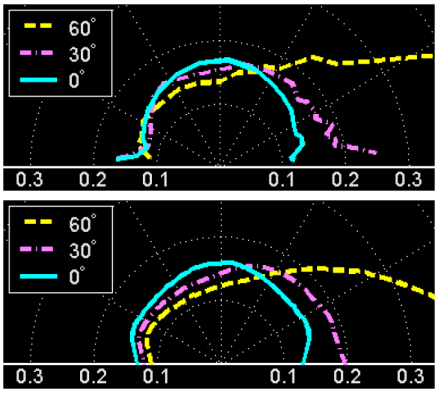

Figure 35: *Comparison of BRDF curves for a lightly pigmented specimen. Top: actual measured BRDF curves provided by Marschner et al. [84]. Bottom: modeled BRDF curves provided by the BioSpec model.*

In these areas the behavior of the transmitted light is near Lambertian, to the point where no internal structure can be noticeable [109].

Finally, we remark that BioSpec is a data driven

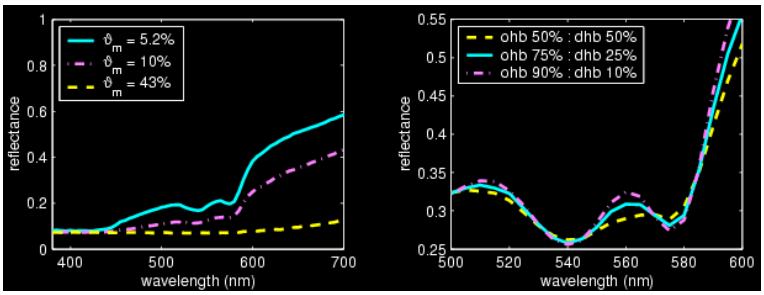

Figure 36: *Comparison of modeled spectral curves provided by the BioSpec model ($\theta_i = 45°$) considering the variation of biological parameters. Left: volume fractions of epidermis occupied by melanosomes (ϑ_m). Right: ratio of oxygenated (ohb) to deoxygenated (dhb) hemoglobin in the dermal layers.*

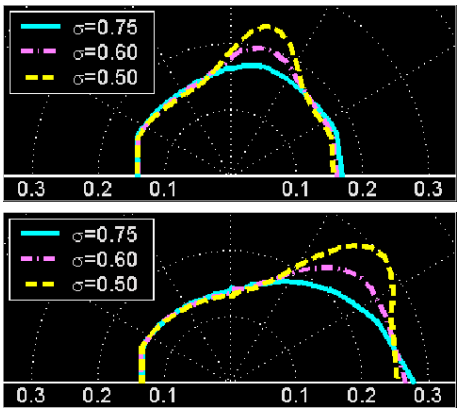

Figure 37: *Comparison of modeled spectral curves provided by the BioSpec model considering variations on the aspect ratio (σ) of the stratum corneum folds. Top: $\theta_i = 15°$. Bottom: $\theta_i = 45°$.*

Figure 38: *Images generated using the BioSpec model to illustrate a spectral simulation jaundice symptoms. Left: $c_{bil} = 0.05g/L$. Center: $c_{bil} = 0.5g/L$. Right: $c_{bil} = 3.0g/L$.*

model. As more data becomes available for the scattering properties of various skin layers or for the spectral properties of additional chromophores, the accuracy of the BioSpec model will increase. However, a lack of data can also result in limiting the skin conditions that can be simulated by this model.

Figure 39: *Images generated using the BioSpec model to illustrate a spectral simulation of erythema conditions. Left: $\vartheta_p = 1.2\%$ and $\vartheta_r = 0.91\%$. Center: $\vartheta_p = 2.7\%$ and $\vartheta_r = 0.3\%$. Right: $\vartheta_p = 3.6\%$ and $\vartheta_r = 0.4\%$.*

9. What's Next?

In this tutorial, we have taken a broad view of the problems related to the simulations of light interaction with human skin. Many questions, however, remain to be answered. In this section, we examine a number of issues related to the improvement and evaluation of such simulations. We also look at more general open problems, their implications and recent developments in applied tissue optics.

9.1. Biological Input Data Availability

Most models of light interaction with organic tissues available in the graphics literature are biologically motivated. Very few models, however, can be classified as biologically-based, *i.e.*, models that incorporate biological data and use algorithms based on the actual biological processes affecting the appearance of these tissues. Although these aspects are essential to establish the predictability of models, their complete fulfillment may present a logistics challenge, since the most appropriate data may not available. For example, to compute spectral reflectance and transmittance for skin specimens, one uses the absorption spectra of various skin pigments which correspond to *in vitro*

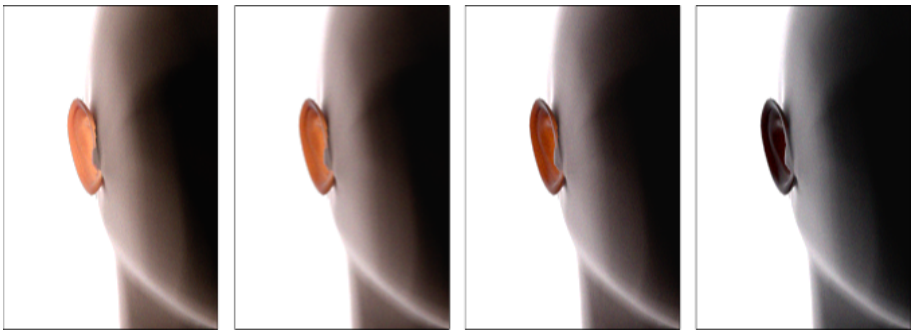

Figure 40: *Images generated using the BioSpec model to show variations in the translucency of skin tissues associated with different levels of melanin pigmentation. From left to right:* $\vartheta_m = 1.9\%$, $\vartheta_m = 5.2\%$ $\vartheta_m = 12\%$ *and* $\vartheta_m = 42\%$.

values, *i.e.,* they are not measured in the tissues, but dissolved in a solvent. The *in vitro* values present spectral shifts with respect to *in vivo* values which are attributed both to the influence of the solvent and to the fact that the pigments inside organic tissues are complexed with other chemical substances such as proteins [62]. Another example refers to refactive indices of organic materials. Ideally, one should use wavelength dependent quantities. In practice, most refractive indices available in the literature correspond to average values. Hence, a key issue that must be addressed to improve the predictability of skin optics simulations is the reliable measurement of biochemical properties, which will likely involve a substantial multidisciplinary effort.

9.2. Accuracy *vs.* Undue Complexity

The current models of light interaction with human skin do not account for the anisotropy*** of human skin, and usually the simulation of shadowing and masking effects is not biologically-based. Although physically-based algorithms for the modeling of these phenomena with respect to inorganic materials have been proposed by computer graphics researchers [46], the generalization of these algorithms to organic materials is not straightforward since the simulation of the underlying biophysical processes involves the whole hierarchy of local illumination, *i.e.*, issues at the microscopic (BRDF) mesoscopic (normal distribution) and macroscopic (geometry) levels need to be addressed. We believe that a careful modeling of skin's geometrical details [132] is essential to achieve a biophysically-based and predictable solution for these questions.

Accuracy and computational time are often conflicting issues in biophysically-based rendering. Although the main goal in this area is the design of accurate and efficient models, sometimes it is difficult to obtain this perfect combination. In order to achieve a higher level of accuracy, it may be necessary to add complexity to a model, which in turn may negatively affect its computational performance. However, this is not always the case. For example, light quickly becomes diffuse after the first interactions in the dermal layers (Section 2.2.2). In this case, a simple cosine distribution would be closer to the actual scattering profile of light transmitted through these layers than the use of the HGPF. Phase functions, such as the HGPF and its variations, were originally used in tissue subsurface scattering simulations to fit data measured at specific wavelengths [19]. Since then, their application has been extended to different organic materials despite the lack of supporting measured data and the fact that their parameters have no biological meaning. As demonstrated in a recent investigation by Baranoski *et al.* [8], the use of a data oriented approach instead of the HGPF increases the accuracy/time ratio of algorithmic subsurface scattering simulations, and contributes to their predictability since the simulations are not controlled by arcane parameters.

9.3. Evaluation and Comparison Data Availability

Usually models of light interaction with matter are evaluated by visually inspecting the images generated using such models. Clearly, such an evaluation may be biased by factors not directly related to the model. For example, the use of a high resolution geometric model

*** In the context of this tutorial, anisotropy refers to the phenomenon observed when the material is rotated around its normal while the light and the viewer directions remain unchanged, and the light intensity reflected to the viewer varies.

of the body part being rendered [129, 66], the application of texture maps, and a careful post-processing spectral tone reproduction [13] may improve the realistic appearance of rendered skin (Figure 41). These aspects, however, correspond to different stages of the rendering pipeline which should be evaluated independently.

A current trend is to perform comparisons between model readings and measured data so that the models can be used in a predictive manner [52]. For example the BioSpec model was tested as a separated unit of the rendering pipeline and the results were compared with actual measured data [40, 84, 150]. These comparisons were performed using a virtual spectrophotometer and a virtual goniophotometer (Section 2), and reproducing the actual measurement conditions as faithfully as possible.

This evaluation approach, however, is bounded by the availability of measured data. As mentioned earlier, skin reflectance and transmittance curves can be found in the biomedical literature, but they are usually restricted to a narrow range of measurement conditions. Furthermore, high fidelity comparisons of measured and modeled quantities require both qualitative and quantitative characterization data for the specimen at hand. Usually only qualitative characterization data is available for skin specimens used in tissue optics experiments. In terms of goniometric (BRDF and BTDF) curves, despite efforts of computer graphics researchers [30, 82, 84, 83], there is still a shortage of data, and the available data sets present the same limitations outlined for the reflectance and transmittance data sets. The lack of measured data is even more serious with respect to subsurface scattering since, to the best of our knowledge, the only relatively reliable data set corresponds to the measurements performed by Bruls and van der Leun [19], which are limited to two wavelengths in the visible range. Therefore, substantial efforts should be also directed towards the reliable measurement of multispectral surface and subsurface skin data.

9.4. Biomedical Applications

As mentioned earlier, computer simulations can assist the visual diagnosis of different skin conditions and diseases [138], including skin tumors [29, 28], and the indirect (noninvasive) measurement of the optical properties of skin tissues. These applications involve the non-iterative and the iterative use of a theoretical model of light interaction with these tissues [24]. The non-iterative approach consists in inverting the model (Section 4). In an iterative approach, the optical properties are implicitly related to measured quantities (*e.g.*, reflectance and transmittance). The model is then run iteratively until these quantities are matched. Clearly, the predictability of these simulations is tied to the accuracy of the model being used. This aspect emphasizes the importance of evaluating the models both qualitatively and quantitatively. This tutorial has shown that no single model is superior in all aspects involved in the simulation of light interaction with human skin, and very few models have been properly evaluated. Hence, there is still room for improvement in this area.

Besides tackling the limitations of the current computer graphics models and improving their evaluation methodology, it will also be necessary to incorporate time dependent mechanisms of photon reemission in their formulation, and to extend their space of parameters to regions of the light spectrum outside the visible domain. Important biophysical processes are triggered by radiation hitting the skin at these wavelengths (Section 3.4).

10. Conclusion

In this tutorial, we presented an overview of the state of the art in the simulation of light interaction with human skin from a computer graphics perspective. Although that are several aspects beyond the scope of this work, such as geometrical modeling and tone reproduction, that also affect the realistic appearance of virtual humans, we believe that the predictability of rendering frameworks can be increased by bringing more biological knowledge and data to bear on the modeling of light interaction with organic materials. Such an approach will likely extend the range of scientific applications of computer graphics algorithms as appropriately suggested by by Donald Greenberg in his Steve Coons Award speech [51]:

> *If computer graphics is to have a role in improving the future of our civilization, the real value will be in its application to science, engineering and design.*

Acknowledgements

Thanks are due to the anonymous reviewers of our tutorial proposal for their useful insights, and to Pat Hanrahan, Jos Stam and Henrik Wann Jensen for graciously allowing us to use their images. The authors are also grateful for funding through the National Sciences and Engineering Council of Canada (NSERC Grant 238337) and the Canada Foundation for Innovation (CFI Project 6218).

Figure 41: *Sequence of images illustrating a process used to create a digital human face. Top row, from left to right: 3D mesh obtained using 3D scanning (close-up of nostril), color data obtained using photographs, and diffuse rendering. Bottom row, from left to right: oily layer rendered using the Torrance and Sparrow model [134]), subsurface scattering simulated using D-T model [67], and the final result with eyebrows and eyelashes rendered using Kajiya and Kay model for hair [69]. (Courtesy of Henrik Wann Jensen).*

References

[1] S. Alaluf, U. Heinrich, W. Stahl, H. Tronnier, and S. Wiseman. Dietary carotenoids contribute to normal human skin color and uv photosensitivity. *Journal of Nutrition*, 132:399–403, 2002. 10

[2] R.R. Anderson and J.A. Parrish. The optics of human skin. *Journal of Investigative Dermatology*, 77(1):13–19, 1981. 9, 11, 13, 14

[3] Elli Angelopoulou. Understanding the color of human skin. In *Human Vision and Electronic Imaging VI*, pages 243–251. SPIE, vol. 4299, 2001. 10, 30, 32

[4] ANSI. Nomenclature and definitions for illuminating engineering. In *ANSI/IES RP-6-1986*. Illuminating Engineering Society of North America, New York, 1986. 8, 9

[5] J.R. Arvo. *Analytic Methods for Simulated Light Transport*. PhD thesis, Yale University, 1995. 2, 3

[6] G.V.G. Baranoski and A. Krishnaswamy. An introduction to light interaction with human skin. *Revista de Informática Teórica e Aplicada*, 11:33–62, 2004. 27

[7] G.V.G. Baranoski, A. Krishnaswamy, and B. Kimmel. An investigation on the use of data-driven scattering profiles in Monte Carlo simulations of ultraviolet light propagation in skin tissues. *Physics in Medicine and Biology*, 49:4799–4809, 2004. 17

[8] G.V.G. Baranoski, A. Krishnaswamy, and B. Kimmel. Increasing the predictability of tissue subsurface scattering simulations. *The Visual Computer*, 21(4):265–278, May 2005. 17, 20, 27, 35

[9] G.V.G. Baranoski and J.G. Rokne. An algorithmic reflectance and transmittance model for plant tissue. *Computer Graphics Forum (EUROGRAPHICS Proceedings)*, 16(3):141–150, September 1997. 29, 31

[10] G.V.G. Baranoski and J.G. Rokne. *Light Interaction with Plants: A Computer Graphics Perspective*. Horwood Publishing, Chichester, UK, 2004. 2, 14, 17

[11] W.W. Barkas. Analysis of light scattered from a surface of low gloss into its specular and diffuse components. *Proc. of Physical Society London*, 51:274–295, 1939. 18

[12] J. Barth, J. Cadet, J.P. Césarini, T.B. Fitzpatrick, A. McKinlay, M. Mutzhas, M. Pathak, M. Peak, D. Sliney, and F. Urbach. CIE-134 collection in photobiology and photochemistry. In *TC6-26 report: Standardization of the Terms UV-A1, UV-A2 and UV-B*. Commission International de L'Eclairage, 1999. 12

[13] I.E. Bell and G.V.G. Baranoski. More than RGB: moving toward spectral color reproduction. ACM SIGGRAPH Course Notes, San Diego, CA, July 2002. Course 24. 36

[14] J.L. Bentley. Multidimensional binary search trees used for associative searching. *Comunications of the ACM*, 18(9):509–517, September 1975. 26

[15] E.M. Berry. Diffuse reflection of light from a matt surface. *Journal of the Optical Society of America*, 7(8):627–633, August 1923. 18

[16] J.F. Blinn. Models of light reflection for computer synthesized images. *Computer Graphics (SIGGRAPH Proceedings)*, 11(2):192–198, 1977. 31

[17] C.E. Bohren and D.R. Huffman. *Absorption and Scattering of Light by Small Particles*. John Wiley & Sons, New York, 1983. 5

[18] M. Bouguer. *Traite d'optique sur la gradation de la lumiére*. M. Ábbe de Lacaille, Paris, 1760. 18

[19] W.A.G. Bruls and J.C. van der Leun. Forward scattering properties of human epidermal layers. *Photochem. Photobiol.*, 40:231–242, 1984. 10, 11, 16, 17, 20, 27, 29, 35, 36

[20] R.L. Burden and J.D. Faires. *Numerical Analysis*. PWS-KENT Publishing Company, Boston, fifth edition, 1993. 14

[21] W.L. Butler. Absorption spectroscopy in vivo: Theory and applications. *Annual Review of Plant Physiology*, 15:451–470, 1964. 5

[22] S. Chandrasekhar. *Radiative Transfer*. Dover Publications Inc., New York, 1960. 2, 18, 22, 23

[23] M.R. Chedekel. Photophysics and photochemistry of melanin. In M.R. Chedekel L. Zeise and T.B. Fitzpatrick, editors, *Melanin: Its Role in Human Photoprotection*, pages 11–22, Overland Park, Kansas, USA, 1995. Valdenmar Publishing Company. 2223b. 27

[24] W. Cheong, S.A. Prahl, and A.J. Welch. A review of the optical properties of biological tissues. *IEEE Journal of Quantum Electronics*, 26(12):2166–2185, December 1990. 13, 36

[25] D.Y. Churmakov, I.V. Meglinsky, S.A. Piletsky, and D.A. Greenhalgh. Analysis of skin tissues spatial fluorescence distribution by the Monte Carlo simulation. *Journal of Physics D: Applied Physics*, 36:1722–1728, July 2003. 17

[26] T.F. Coleman and C. an Loan. *Handbook of Matrix Computations*. SIAM Publications, Philadelphia, PA, 1988. 23

[27] R.L. Cook and K.E. Torrance. A reflectance model for computer graphics. *ACM Transactions on Graphics*, 1(1):7–24, January 1982. 22, 23

[28] S.D. Cotton. A noninvasive skin imaging system. Technical Report CSR-97-03, School of Computer Science, The University of Birmingham, 1997. 1, 36

[29] S.D. Cotton and E. Claridge. Developing a predictive model of skin colouring. In *SPIE Vol. 2708, Medical Imaging 1996*, pages 814–825, 1996. 14, 36

[30] K.J. Dana, B. van Ginneken, S.K. Nayar, and J.J. Koenderink. Reflectance and texture of real world surfaces. *ACM Transactions on Graphics*, 18(1):1–34, 1999. 36

[31] B.L. Diffey. A mathematical model for ultraviolet optics in skin. *Physics in Medicine and Biology*, 28(6):647–657, 1983. 14

[32] M. Doi and S. Tominaga. Spectral estimation of human skin color using the Kubelka-Munk theory. In *SPIE/IS&T Electronic Imaging*, pages 221–228. SPIE, vol. 5008, 2003. 9, 10, 14, 15

[33] J.J. Dongarra, J.R. Bunch, C.B. Moler, and G.W. Stewart. *LINPACK Users' Guides*. SIAM Publications, Philadelphia, PA, 1979. 23

[34] C. Donner and H.W. Jensen. Light diffusion in multilayered translucent materials. July 2005. to appear. 28

[35] R.M.P. Doornbos, R. Lang, M.C. Aalders, F.W. Cross, and H.J.C.M. Sterenborg. The determination of in vivo human tissue optical properties and absolute chromophore concentrations using spatially resolved steady-state diffuse reflectance spectroscopy. *Physics in Medicine and Biology*, 44:967–981, 1999. 15

[36] A. Dunn and R. Richards-Kortum. Three-dimensional computation of light scattering from cells. *IEEE Selected Topics in Quantum Electronics*, 2:898–905, 1996. 17

[37] Z. Bai E. Anderson, C. Bischof, S. Blackford, J. Demmel, J. Dongarra, J. Du Croz, A. Greenbaum, S. Hammarling, A. McKenney, and D. Sorensen. *LAPACK Users' Guides*. SIAM Publications, Philadelphia, PA, 3rd edition, 1999. 23

[38] W.G. Eagan and T.W. Hilgeman. *Optical Properties of Inhomogeneous Materials*. Academic Press, New York, NY, 1979. 26

[39] G. Eason, A. Veitch, R. Nisbet, and F. Turnbull. The theory of backscattering of light by blood. *Journal of Physics*, 11:1463–1479, 1978. 15

[40] M.A. Everett, E. Yeargers, R.M. Sayre, and R.L. Olsen. Penetration of epidermis by ultraviolet rays. *Photochemistry and Photobiology*, 5:533–542, 1966. 9, 32, 33, 36

[41] T.J. Farell, M.S. Patterson, and B. Wilson. A diffusion theory model of spatially resolved, steady-state diffuse reflectance for the noninvasive determination of tissue optical properties in vivo. *Medical Physics*, 19:879–888, 1992. 14, 15

[42] T.B. Fitzpatrick and J.L. Bolognia. Human melanin pigmentation: role in pathogenesis of cutaneous melanoma. In M.R. Chedekel L. Zeise and T.B. Fitzpatrick, editors, *Melanin: Its Role in Human Photoprotection*, pages 177–182, Overland Park, Kansas, USA, 1995. Valdenmar Publishing Company. 12

[43] R. Flewelling. Noninvasive optical monitoring. In J.D. Bronzino, editor, *The Biomedical Engineering Handbook*, pages 1–11, Boca Raton, FL, USA, 1981. IEEE Press. Section 86. 10

[44] Stephen T. Flock, Michael S. Patterson, Brian C. Wilson, and Douglas R. Wyman. Monte Carlo modeling of light propagation in highly scattering tissues - I: Model predictions and comparison with diffusion theory. *IEEE Transactions on Biomedical Engineering*, 36(12):1162–1168, December 1989. 15, 27

[45] J. Foley, A. van Dam, S.K. Feiner, and J.F. Hughes. *Computer Graphics: Principles and Practice*. Addison-Wesley Publishing Company, Reading, Massachusetts, second edition, 1990. 26

[46] A. Fournier. From local to global illumination and back. In P. M. Hanrahan and W. Purgathofer, editors, *Rendering Techniques'95 (Proceedings of the Sixth Eurographics Rendering Workshop)*, pages 127–136, Dublin, June 1995. Springer-Verlag. 35

[47] R.J. Fretterd and R.L. Longini. Diffusion dipole source. *Journal of the Optical Society of America*, 63(3):336–337, 1973. 15

[48] K. Furutso. Diffusion equation derived from space-time transport equation. *Journal of the Optical Society of America*, 70:360, 1980. 27

[49] C.F. Gerald and P.O. Wheatley. *Applied Numerical Analysis*. Addison-Wesley, Reading, Massachusetts, 6th edition, 1997. 22, 23

[50] A.S. Glassner. *Principles of Digital Image Synthesis*. Morgan Kaufmann Publishers, Inc, San Francisco, 1995. 2, 3, 4, 8, 17, 28

[51] D.P. Greenberg. 1987 Steven A. Coons Award Lecture. *Computer Graphics*, 22(1):7–14, February 1988. 36

[52] D.P. Greenberg, J. Arvo, E. Lafortune, K.E. Torrance, J.A. Ferwerda, B. Walter, B. Trumbore, P. Shirley, S. Pattanaik, and S. Foo. A framework for realistic image synthesis. In *SIGGRAPH, Annual Conference Series*, pages 477–494, 1997. 36

[53] R.A.J. Groenhuis, H.A. Fewerda, and J.J.T. Bosch. Scattering and absorption of turbid materials determined from reflection measurements. 1: Theory. *Applied Optics*, 22(16):2456–2462, August 1983. 26

[54] P. Hanrahan and W. Krueger. Reflection from layered surfaces due to subsurface scattering. In *SIGGRAPH, Annual Conference Series*, pages 165–174, August 1993. 17, 18, 19, 20, 21, 32

[55] A. Haro, B. Guenter, and I. Essa. Real-time, photorealistic, physically based rendering of fine scale human skin structure. In P. M. Hanrahan and W. Purgathofer, editors, *Rendering Techniques'2001 (Proceedings of the 12th Eurographics Rendering Workshop)*, pages 53–62, London, June 2001. Springer-Verlag. 2

[56] E Hecht and A. Zajac. *Optics*. Addison-Wesley, Reading, Massachusetts, 1974. 2, 3, 29

[57] L.G. Henyey and J.L. Greenstein. Diffuse radiation in the galaxy. *Astrophysics Journal*, 93:70–83, 1941. 6

[58] R.J. Hirko, R.J. Fretterd, and R.L. Longini. Application of the diffusion dipole to modelling the optical characteristics of blood. *Medical and Biological Engineering*, 3:192–195, March 1975. 15

[59] R.S. Hunter and R.W. Harold. *The Measurement of Appearance*. John Wiley & Sons, New York, second edition, 1987. 3, 7

[60] A. Ishimaru. *Wave Propagation and Scattering in Random Media*, volume 1. IEEE Press, New York, 2nd edition, 1978. 5, 6, 14

[61] S. Jacquemoud and S.L. Ustin. Leaf optical properties: A state of the art. In *8th International Symposium of Physical Measurements & Signatures in Remote Sensing*, pages 223–332, Aussois, France, January 2001. CNES. 17

[62] S. Jacquemoud, S.L. Ustin, J. Verdebout, G. Schmuck, G. Andreoli, and B. Hosgood. Estimating leaf biochemistry using prospect leaf optical properties model. *Remote Sensing of Environment*, 56:194–202, 1996. 32, 35

[63] S.L. Jacques. Origins of tissue optical properties in the uva visible and nir regions. *OSA TOPS on Advances in Optical Imaging and Photon Migration*, 2:364–369, 1996. 9, 10, 12, 30

[64] S.L. Jacques, C.A. Alter, and S.A. Prahl. Angular dependence of HeNe laser light scattering by human dermis. *Lasers in Life Sciences*, 1(4):309–333, 1987. 11, 16

[65] H.W. Jensen and J. Buhler. A rapid hierarchical rendering technique for translucent materials. In *SIGGRAPH, Annual Conference Series*, pages 576–581, July 2002. 24, 25, 26, 27

[66] H.W. Jensen and J. Buhler. Digital face cloning. In M.R. Chedekel L. Zeise and T.B. Fitzpatrick, editors, *SIGGRAPH'2003 Technical Sketches*, pages 11–22, Overland Park, Kansas, USA, 2003. Valdenmar Publishing Company. 2223b. 25, 36

[67] H.W. Jensen, S.R. Marschner, M. Levoy, and P. Hanrahan. A practical model for subsurface light transport. In *SIGGRAPH, Annual Conference Series*, pages 511–518, August 2001. 24, 25, 26, 27, 32, 37

[68] Z. Jin and K. Stammes. Radiative transfer in nonuniformly refracting layered media: atmosphere-ocean system. *Applied Optics*, 33(3):431–442, January 1994. 22

[69] J. Kajiya and T. Kay. Rendering fur with three dimensional textures. *Computer Graphics (SIGGRAPH Proceedings)*, 23(3):271–280, July 1989. 37

[70] G.W. Kattawar. A three-parameter analytic phase function for multiple scattering calculations. *Journal of Quantitative Spectroscopy and Radiative Transfer*, 15:839–849, 1975. 7

[71] G. Kelfkens and J.C van der Leun. Skin temperature changes after irradiation with UVB or UVC: implications for the mechanism underlying ultraviolet erythema. *Physics in Medicine and Biology*, 34(5):599–608, 1989. 12

[72] C. Kolb. *Rayshade User's Guide and Reference Manual*. Princeton University, January 1992. 19

[73] N. Kollias. The spectroscopy of human melanin pigmentation. In M.R. Chedekel L. Zeise and T.B. Fitzpatrick, editors, *Melanin: Its Role in Human Photoprotection*, pages 31–38, Overland Park, Kansas, USA, 1995. Valdenmar Publishing Company. 12

[74] A. Krishnaswamy. BioSpec: A biophysically-based spectral model of light interaction with human skin. Master's thesis, School of Computer Science, University of Waterloo, Waterloo, Ontario, Canada, 2005. 29, 30, 31, 32

[75] A. Krishnaswamy and G.V.G. Baranoski. A biophysically-based spectral model of light interaction with human skin. *Computer Graphics Forum (EUROGRAPHICS Proceedings)*, 23(3):331–340, 2004. 28, 29, 31, 32, 33

[76] P. Kubelka and F. Munk. Ein beitrag zur optik der farbanstriche. *Zurich Tech. Physik*, 12:543, 1931. 13

[77] R. Lee, M.M. Mathews-Roth, M.A. Pathak, and J.A. Parrish. The detection of carotenoid pigments in human skin. *Journal of Investigative Dermatology*, 64:175–177, 1975. 10

[78] G.N. Lewis. The conservation of photons. *Nature*, 2981(118):874–875, December 1926. 2

[79] R.S. Longhurst. *Geometrical and Physical Optics*. Longman Group Limited, London, third edition, 1973. 2, 3, 8

[80] D.L. MacAdam. *Color Measurements Theme and Variations*. Springer Verlag, Berlin, 1981. 8

[81] S.R. Marschner, H.W. Jensen, M. Cammarano, S. Worley, and P. Hanrahan. Light scattering from human hair fibers. *ACM Transactions on Graphics*, 22(3):780–791, 2003. 2

[82] S.R. Marschner, S. H. Westin, E.P.F. Lafortune, K.E. Torrance, and D.P. Greenberg. Image-based brdf measurement. Technical Report PCG-99-1, Program of Computer Graphics, Cornell University, USA, January 1999. 36

[83] S.R. Marschner, S. H. Westin, E.P.F. Lafortune, K.E. Torrance, and D.P. Greenberg. Image-based brdf measurement including human skin. In D. Lischinski and G. W. Larson, editors, *Rendering Techniques'1999 (Proceedings of the 10th Eurographics Rendering Workshop)*, pages 119–130, Granada, June 1999. Springer-Verlag. 36

[84] S.R. Marschner, S. H. Westin, E.P.F. Lafortune, K.E. Torrance, and D.P. Greenberg. Reflectance measurements of human skin. Technical Report PCG-99-2, Program of Computer Graphics, Cornell University, USA, January 1999. 32, 33, 36

[85] E.J. McCartney. *Optics of the Atmosphere: Scattering by Molecules and Particles*. John Wiley & Sons Inc., 1976. 4, 29, 30

[86] I.V. Meglinsky and S.J. Matcher. Modelling the sampling volume for skin blood oxygenation. *Medical & Biological Engineering & Computing*, 39:44–49, 2001. 9, 17

[87] I.V. Meglinsky and S.J. Matcher. Computer simulation of the skin reflectance spectra. *Computer Methods and Programs in Biomedicine*, 70:179–186, 2003. 17

[88] D.H. Menzel. *Selected Papers on the Transfer of Radiation*. Dover Publications, New York, 1966. 2

[89] N. Metropolis and S. Ulam. The Monte Carlo method. *Journal of the American Statistical Association*, 44(247):335–341, September 1949. 16

[90] J.R. Meyer-Arendt. *Introduction to Modern and Classical Optics*. Prentice-Hall, New Jersey, 1984. 2, 8

[91] J.R. Mourant, J.P. Freyer, A.H. Hielscher, A.A. Eick, D. Shen, and T.M. Johnson. Mechanisms of light scattering from biological cells relevant to noninvasive optical-tissue diagnostics. *Applied Optics*, 37(16):3586–3593, June 1998. 17

[92] H. Nakai, Y. Manabe, and S. Inokuchi. Simulation analysis of spectral distributions of human skin. In *14th International Conference on Pattern Recognition*, pages 1065–1067, 1998. 17

[93] C.S. Ng and L. Li. A multi-layered reflection model of natural human skin. In *Computer Graphics International 2001*, pages 249–256, Hong Kong, July 2001. 20, 32

[94] F.E. Nicodemus, J.C. Richmond, J.J. Hsia, I.W. Ginsberg, and T. Limperis. Geometrical considerations and nomenclature for reflectance. In L.B. Wolff, S.A. Shafer, and G.E. Healey, editors, *Physics-Based Vision Principles and Practice: Radiometry*, pages 94–145, Boston, 1992. Jones and Bartlett Publishers. 8, 23

[95] S.K. Nilsson. Skin temperature over an artificial heat source implanted in man. *Physics in Medicine and Biology*, 20(3):366–383, 1975. 12

[96] M. Nischik and C. Forster. Analysis of skin erythema using true-color images. *IEEE Transactions on Medical Imaging*, 16(6):711–716, December 1997. 1

[97] S.E. Orchard. Reflection and transmission of light by diffusing suspensions. *Journal of the Optical Society of America*, 59:1584–1597, 1969. 26

[98] R.D. Overhem and D.L. Wagner. *Light and Color*. John Wiley & Sons, New York, N.Y., 1982. 3

[99] K.F. Palmer and D. Williams. Optical properties of water in the near infrared. *Journal of the Optical Society of America*, 64(8):1107–1110, August 1974. 8

[100] D. Parsad, K. Wakamatsu, A.J. Kanwar, B. Kumar, and S. Ito. Eumelanin and phaeomelanin contents of depigmented and repigmented skin in vitiligo patients. *British Journal of Dermatology*, 149:624–626, 2003. 9

[101] M.A. Pathak. Functions of melanin and protection by melanin. In M.R. Chedekel L. Zeise and T.B. Fitzpatrick, editors, *Melanin: Its Role in Human Photoprotection*, pages 125–134, Overland Park, Kansas, USA, 1995. Valdenmar Publishing Company. 12

[102] A. Pearce and K. Sung. Maya software rendering: A technical overview. Technical Report AP-M-SWR-01, Alias—Wavefront, Toronto, Canada, 1998. 23

[103] S.A. Prahl. *Light Transport in Tissue*. PhD thesis, The University of Texas at Austin, TX, USA, December 1988. 5, 6, 15, 16, 18, 22, 23

[104] S.A. Prahl, M. Keijzer, S.L. Jacques, and A.J. Welch. A Monte Carlo model of light propagation in tissue. *SPIE Institute Series*, IS 5:102–111, 1989. 16, 17, 18, 29

[105] S.A. Prahl, M.J.C. van Gemert, and A.J. Welch. Determining the optical properties of turbid media using the adding-doubling method. *Applied Optics*, 32(4):559–568, 1993. 15, 16

[106] R.W. Preisendorfer. *Radiative Transfer on Discrete Spaces*. Pergamon, New York, N.Y., 1965. 2

[107] S. Premoze. Analytic light transport approximations for volumetric materials. In *Proceedings of the 10th Pacific Conference on Computer Graphics and Applications - Pacific Graphics'2002*, pages 48–57, Beijing, October 2002. 2

[108] S. Premoze, M. Ashikhmin, and P. Shirley. Path integration for light transport in volumes. In P. Christensen and D. Cohen-Or, editors, *Eurographics Symposium on Rendering*, pages 75–84, 2003. 6

[109] J. Rodriguez, I.V. Yaroslavsky, A.N. Yaroslavsky, H. Battarbee, and V.V. Tuchin. Time-resolved imaging in diffusive media. In V.V. Tuchin, editor, *Handbook of Optical Biomedical Diagnostics*, pages 357–404, Bellingham, WA, USA, 2002. SPIE Press. 33

[110] W. Ruhle and A. Wild. The intensification of absorbance changes in leaves by light-dispersion. differences between high-light and low-light leaves. *Planta*, 146:551–557, 1979. 5

[111] I.S. Saidi. *Transcutaneous optical measurement of hyperbilirubinemia in neonates*. PhD thesis, Rice University, Houston, Texas, USA, 1994. 30

[112] D.K. Sardar and L.B. Levy. Optical properties of whole blood. *Lasers in Medical Science*, 13:106–111, 1998. 15

[113] J.M. Schmitt, G.X. Zhou, E.C. Walker, and R.T. Wall. Multilayer model of photon diffusion in skin. *Journal of the Optical Society of America*, 7(11):2141–2153, November 1990. 14

[114] A. Schuster. Radiation through foggy atmosphere. *Astrophysical Journal*, 21(1):1–22, January 1905. 2

[115] F.W. Sears, M.W. Zemansky, and H.D. Young. *College Physics Part I Mechanics, Heat and Sound*. Addison-Wesley Publishing Company, Reading, Massachusetts, fourth edition, 1974. 12

[116] H. Seeliger. The photometry of diffusely reflecting surfaces. *Koniglich Bayerische Akademie der Wissenschaften*, 18:201–248, 1888. (in German). 18

[117] M. Shimada, Y. Yamada, M. Itoh, and T. Yatagai. Melanin and blood concentration in human skin studied by multiple regression analysis: assessment by Monte Carlo simulation. *Physics in Medicine and Biology*, 46:2397–2406, 2001. 17

[118] P. Shirley. Physically based lighting calculations for computer graphics: A modern perspective. In K. Bouatouch and C. Bouville, editors, *Eurographics Workshop on Photosimulation, Realism and Physics in Computer Graphics*, pages 67–81, Amsterdam, June 1990. Elsevier. 9

[119] P. Shirley. *Physically Based Lighting for Computer Graphics*. PhD thesis, Dept. of Computer Science, University of Illinois, November 1990. 3, 5, 9

[120] P. Shirley, G.V.G. Baranoski, B.S. Cho, A. Defrancesco, V. Gupta, B. Jones, R. Kamath, J. Kim, K. Kim, T. Loos, H. Ma, C. Meyer, D. Rusinov, S. Sampson, G. Vogl, B. Winnicka, and K. Zimmerman. *The GG Library Reference Manual*. Department of Computer Science, Indiana University, Bloomington, Indiana, USA, 1993. 31

[121] P. Shirley and K. Sung. A ray tracing framework for global illumination systems. In *Graphics Interface*, pages 117–128, Toronto, 1991. Canadian Information Processing Society. 31

[122] C.R. Simpson, M. Kohl, M. Essenpreis, and M. Cope. Near infrared optical properties of ex-vivo human skin and subcutaneous tissues measured using the Monte Carlo inversion technique. *Physics in Medicine and Biology*, 43:2465–2478, 1998. 17

[123] H. Smith and D.C. Morgan. The spectral characteristics of the visible radiation incident upon the surface of the earth. In H. Smith, editor, *Plants and the Daylight Spectrum*, pages 3–20, London, January 1981. Academic Press. 4

[124] J. Stam. An illumination model for a skin layer bounded by rough surfaces. In P. M. Hanrahan and W. Purgathofer, editors, *Rendering Techniques'2001 (Proceedings of the 12th Eurographics Rendering Workshop)*, pages 39–52, London, June 2001. Springer-Verlag. 21, 22, 23, 32

[125] K. Stamnes and P. Conklin. A new multi-layer dis-

crete ordinate approach to radiative transfer in vertically inhomogeneous atmospheres. *Journal of Quantum Spectroscopy and Radiative Transfer*, 31(3):273–282, 1984. 22

[126] K. Stanzl and L. Zastrow. Melanin: an effective photoprotectant against UV-A rays. In M.R. Chedekel L. Zeise and T.B. Fitzpatrick, editors, *Melanin: Its Role in Human Photoprotection*, pages 59–63, Overland Park, Kansas, USA, 1995. Valdenmar Publishing Company. 12

[127] J.M. Steinke and A.P. Shepherd. Diffusion model of the optical absorbance of whole blood. *Journal of the Optical Society of America*, 5(6):813–822, 1988. 15

[128] Y. Su, W. Wang, K. Xu, and C. Jiang. The optical properties of skin. In *Optics in Health Care and Biomedical Optics: Diagnostics and Treatment*, pages 299–304. SPIE, vol. 4916, 2002. 10

[129] J.L. Swerdlow. Unmasking skin. *National Geographic*, pages 36–63, November 2002. 1, 36

[130] P.S. Talreja, G.B. Kasting, N.K. Kleene, W.L. Pickens, and T. Wang. Visualization of the lipid barrier and measurement of lipid pathlength in human stratum corneum. *AAPS PharmSCi*, 3(2):1–9, 2001. 9, 10, 33

[131] J. Tessendorf and D. Wilson. Impact of multiple scattering on simulated infrared clod scene images. In P. Christensen and D. Cohen-Or, editors, *SPIE. Characterization and Propagation of Sources and Backgrounds*, pages 75–84, 1994. 2223b. 6

[132] N. Thalmann, P. Kalra, J.L. Lévêque, R. Bazin, D. Batisse, and B. Querleux. A computational skin model: fold and wrinkle formation. *IEEE Transactions on Information Technology in Biomedicine*, 6(4):317–323, 2002. 10, 33, 35

[133] A.J. Thody, E.M. Higgins, K. Wakamatsu, S. Ito, S.A. Burchill, and J.M. Marks. Pheomelanin as well as eumelanin is present in human dermis. *Journal of Investigative Dermatology*, 97:340–344, 1991. 9

[134] K.E. Torrance and E.M. Sparrow. Theory for off-specular reflection from roughned surfaces. *Journal of the Optical Society of America*, 57(9):1105–1114, 1967. 18, 20, 25, 37

[135] T.S. Trowbridge and K.P. Reitz. Average irregularity representation of a rough surface for ray reflection. *Journal of the Optical Society of America*, 65(5):531–536, May 1975. 29, 31

[136] N. Tsumura, M. Kawabuchi, H. Haneishi, and Y. Miyabe. Mapping pigmentation in human skin by multi- visible-spectral imaging by inverse optical scattering technique. In *IS&T/SID Eighth Color Imaging Conference*, pages 81–84, 2000. 13, 17

[137] N. Tsumura, N. Ojima, K. Sato, M. Shiraishi, H. Shimizu, H. Nabeshima, S. Akazaki, K. Hori, and Y. Miyake. Image-based skin color and texture analysis/synthesis by extracting hemoglobin and melanin information in the skin. In *SIGGRAPH, Annual Conference Series*, 2003. 2

[138] V.V. Tuchin. *Tissue Optics Light Scattering Methods and Instruments for Medical Diagnosis*. The International Society for Optical Engineering, Bellingham, WA, USA, 2000. 9, 10, 13, 16, 36

[139] V.V. Tuchin, S.R. Utz, and I.V. Yaroslavsky. Tissue optics, light distribution, and spectroscopy. *Optical Engineering*, 33:3178–3188, 1994. 13, 14

[140] A. Uesugi, W.M. Irvine, and Y. Kawata. Formation of absorption spectra by diffuse reflection from a semi-infinite planetary atmosphere. *Journal of Quantitative Spectroscopy and Radiative Transfer*, 11:797–808, 1971. 7

[141] H.C. van de Hulst. *Multiple Light Scattering: Tables, Formulas, and Applications*, volume 1. Academic Press, New York, 1980. 15, 16, 23

[142] H.C. van de Hulst. *Multiple Light Scattering: Tables, Formulas, and Applications*, volume 2. Academic Press, New York, 1980. 23

[143] H.C. van de Hulst. *Light Scattering by Small Particles*. Dover Publications Inc., New York, 2nd edition, 1981. 5, 6

[144] J.C. van der Leun. *Ultraviolet Erythema*. PhD thesis, University of Utrecht, The Netherlands, 1966. 12

[145] M.J.C. van Gemert, S.L. Jacques, H.J.C.M. Sterenborg, and W.M. Star. Skin optics. *IEEE Transactions on Biomedical Engineering*, 36(12):1146–1154, 1989. 10, 14, 17, 19, 27

[146] M.J.C. van Gemert and W.M. Star. Relations between the Kubelka-Munk and the transport equation models for anisotropic scattering. *Laser in the Life Sciences*, 1(4):287–298, 1987. 13, 14

[147] M.J.C. van Gemert, A.J. Welch, and W.M. Star. Tissue optics for a slab geometry in diffusion approximation. *Laser in the Life Sciences*, 2:295–302, 1987. 14, 15, 27

[148] B. van Ginneken, M. Stavridi, and J.J. Koenderink. Diffuse and specular reflectance from rough surfaces. *Applied Optics*, 37(1):130–139, 1998. 22, 23

[149] T.C. Vogelmann. Plant tissue optics. *Annual Review of Plant Physiology and Plant Molecular Biology*, 44:231–251, 1993. 5

[150] M.J. Vrhel, R. Gershon, and L.S. Iwan. Measurement and analysis of object reflectance spectra. *Color Research and Application*, 19(1):4–9, 1994. 32, 36

[151] S. Wan, R. Anderson, and J.A. Parrish. Analytical modeling for the optical properties of the skin with in vitro and in vivo appplications. *Photochemistry and Photobiology*, 34:493–499, 1981. 13, 14

[152] L. Wang and S.L. Jacques. Hybrid method of Monte

Carlo simulation and diffusion theory for light reflectance by turbid media. *Optical Society of America*, 10(8):1746–1752, 1995. 14, 16

[153] S.J. Williamson and H.Z. Cummins. *Light and Color in Nature and Art*. John Wiley & Sons, New York, 1983. 4

[154] B.C. Wilson and G. Adam. A Monte Carlo model for the absorption and flux distributions of light in tissue. *Medical Physics*, 10:824–830, 1983. 16

[155] A.N. Witt. Multiple scattering in reflection nebulae. I. a Monte Carlo approach. *The Astrophysical Journal Supplement Series*, 15:1–6, September 1977. 6, 7, 16

[156] A.N. Yaroslavsky, A.V. Priezzhev, J. Rodriguez, I.V. Yaroslavsky, and H. Battarbee. Optics of blood. In V.V. Tuchin, editor, *Handbook of Optical Biomedical Diagnostics*, pages 169–216, Bellingham, WA, USA, 2002. SPIE Press. 10

[157] A.N. Yaroslavsky, S.R. Utz, S.N. Tatarintsev, and V.V. Tuchin. Angular scattering properties of human epidermal layers. In *Human Vision and Electronic Imaging VI*, pages 38–41. SPIE, vol. 2100, 1994. 13, 14

[158] G. Yoon. *Absorption and Scattering of Laser Light in Biological Media - Mathematical Modeling and Methods for Determining Optical Properties*. PhD thesis, University of Texas at Austin, USA, 1988. 13, 14

[159] G. Yoon, S.A. Prahl, and A.J. Welch. Accuracies of the diffusion approximation and its similarity relations for laser irradiated biological media. *Applied Optics*, 28(12):2250–2255, 1989. 15, 27

[160] G. Yoon, A.J. Welch, M. Motamedi, and M.C.J. van Gemert. Development and application of three-dimensional light distribution model for laser irradiated tissue. *IEEE Journal of Quantum Electronics*, QE-23:1721–1733, 1987. 13, 14, 16

[161] G. Zonios, J. Bykowsky, and N. Kollias. Skin melanin, hemoglobin, and light scattering properties can be quantitatively assessed in vivo using diffuse reflectance spectroscopy. *Journal of Investigative Dermatology*, 117(6):1452–1457, 2001. 13, 32